NASA Contractor Report 4616

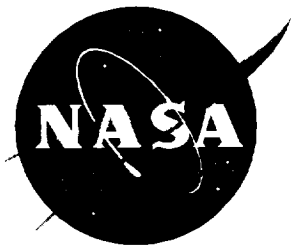

Near Minimum-Time Maneuvers of the Advanced Space Structures Technology Research Experiment (ASTREX) Test Article: Theory and Experiments

Srinivas R. Vadali and Michael T. Carter
Texas A&M University • College Station, Texas

National Aeronautics and Space Administration
Langley Research Center • Hampton, Virginia 23681-0001

Prepared for Langley Research Center
under Contract NAS1-19373

August 1994

ABSTRACT

Near Minimum-Time Maneuvers of the
Advanced Space Structures Technology Research Experiment
(ASTREX) Test Article:
Theory and Experiments

The Phillips Laboratory at the Edwards Air Force Base has developed the Advanced Space Structures Technology Research Experiment (ASTREX) facility to serve as a testbed for demonstrating the applicability of proven theories to the challenges of spacecraft maneuvers and structural control. This report describes the work performed on the ASTREX test article by Texas A&M University under contract NAS1-19373 as a part of the Control-Structure Interaction (CSI) Guest Investigator Program. The focus of this work is on maneuvering the ASTREX test article with compressed air thrusters that can be throttled, while attenuating structural excitation. The theoretical foundation for designing the near minimum-time thrust commands is based on the generation of smooth, parameterized optimal open-loop control profiles, and the determination of control laws for final position regulation and tracking using Lyapunov stability theory. Details of the theory, mathematical modeling, model updating and compensation for the presence of "real world" effects are described and the experimental results are presented. The results show an excellent match between theory and experiments. Considerable leakage of the compressed air supply limited the "size" of the maneuvers and also adversely affected the fine-pointing accuracy.

ACKNOWLEDGEMENTS

The authors would like to thank Dr. Alok Das of the Phillips Laboratory, Kirtland Air Force Base, for his support on this project. Dr. Nandu S. Abhyankar of DYNACS, Inc. has provided excellent technical assistance and specific ASTREX information which have made these complex experiments much easier to implement. We also thank Dr. Tarunraj Singh, Dr. John L. Junkins, Mark Bell, and Dr. Thomas C. Pollock for many interesting discussions and key insights. Ms. Rudeen Smith-Taylor of NASA Langley Research Center, the technical monitor, has been extremely helpful in providing us with continuous support throughout the duration of the project.

TABLE OF CONTENTS

LIST OF FIGURES

LIST OF TABLES

1.0. INTRODUCTION

Optimal large-angle maneuvering of rigid and flexible spacecraft has been a topic of interest for more than a decade.[1-8] Many current and future spacecraft require rapid large-angle maneuvering with vibration suppression during and after the maneuvers. Control designers are faced with the challenging problem of Control-Structure Interaction (CSI) due to increasing size-to-weight ratios and rapid maneuvering and precision pointing requirements. This report presents the activities of Texas A&M University under the Phase II NASA/DOD CSI Guest Investigator Program. The primary focus of this work was to demonstrate experimentally some of the significant theoretical advances on the design of control laws for maneuvering large space structures. The ground test facility selected for this purpose was the Advanced Space Structures Technology Research Experiment (ASTREX) facility developed by the Air Force Phillips Laboratory at the Edwards Air Force Base.

The techniques implemented on the test article were near minimum-time open-loop control with torque smoothing and Lyapunov final position regulation and tracking control. The connection of the primary structure to the support pedestal with a slight center of gravity (c.g.) offset from the pivot point resulted in a very low frequency pendulum mode at approximately 0.05 Hz besides numerous structural modes in the range of 3.5-50 Hz. In order to reduce the complexity of the control laws, the control design was based on a rigid body model but torque-smoothing was used to minimize structural excitation. The actuators available for maneuvering were compressed air thrusters that could be throttled to produce continuously-varying thrust. Although rate sensors were available for use, their low frequency characteristics made them unsuitable for providing rigid body rates. The feedback control laws were implemented using attitude measurements and rates were estimated by filtering the attitude measurements.

Considerable leakage in the plumbing of the thruster system prevented "large" maneuvers from being performed. Furthermore, stray voltages in the control electronics produced erratic thruster firings leading to unacceptably large motions of the structure. To avoid possible damage to the structure, the maximum input voltage was limited, which consequently limited the "size" of the maneuvers. In spite of these difficulties, the control laws worked remarkably well, as shown in the experimental results.

This report begins with the description of the ASTREX test structure, its subsystems and the governing equations of motion for its dynamics in Section 2.0. Section 3.0 presents the parameterization and optimization algorithm for the open-loop control, as well as the design and

the computational aspects for the Lyapunov-based control laws. Section 4.0 describes the initial open-loop control experiments, model refinement, and the results obtained based on the refined model. Section 5.0 presents the feedback control experiments that include final position regulation and tracking control laws to achieve fine pointing. The authors' concluding remarks and suggestions for future work are presented in Section 6.0.

2.0. THE ASTREX TEST ARTICLE

The ASTREX (Advanced Space Structures Technology Research Experiment) test article at Phillips Laboratory, Edwards AFB, CA, is a dynamically-scaled structural model of a 3-mirror space-based laser beam expander. Its mass is approximately 4106 kg (9033 lb).[9] The test article is balanced on a three-axis air-bearing system that applies a 100 psi compressed airflow cushion under a hemispherical ball mounted at the top of a 5-meter vertical pedestal. Figure 2.1 shows a diagram of the test article which denotes its components and three major sections:

1. The *Primary Structure* is a 5.5-meter diameter truss that includes six sets of steel plates mounted on its face to simulate the primary mirror and two cylindrical masses mounted on its sides to simulate tracker telescopes. Both the thrusters and the control moment gyros (CMGs) are mounted on this structure.

2. The *Secondary Structure* is a triangular structure which houses the reaction wheel actuator and the masses designed to simulate the secondary mirror. The Secondary Structure is attached to the Primary Structure with a tripod formation of three 5.1-meter graphite epoxy tubes. These graphite-epoxy tubes were designed by TRW with embedded sensors and actuators for vibration suppression.

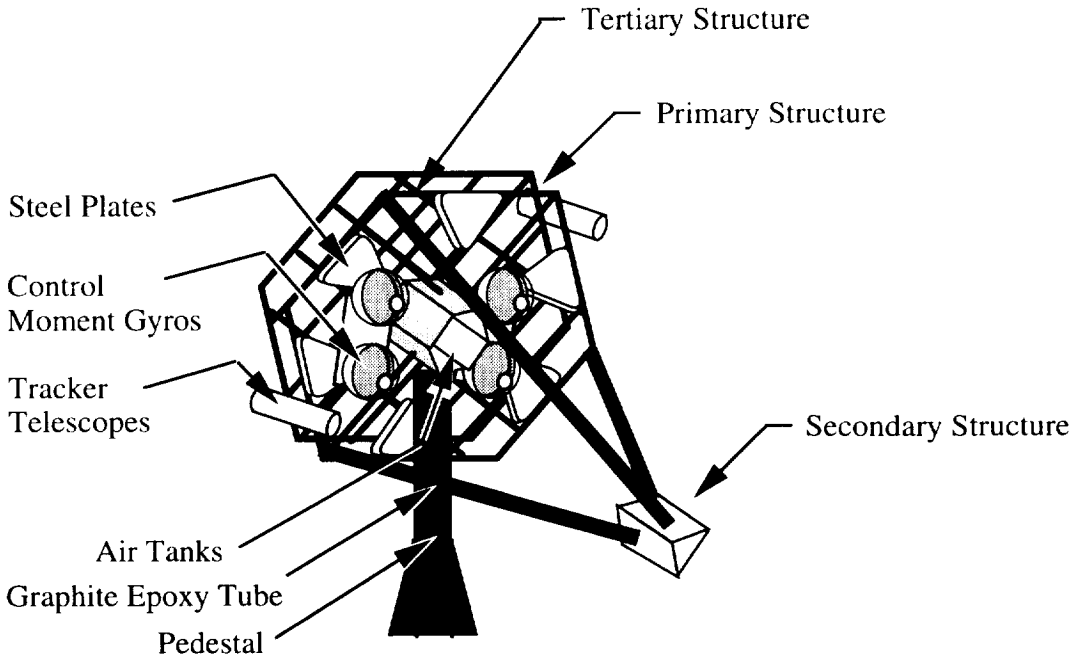

Figure 2.1. Components of the ASTREX Structure

3. The *Tertiary Structure* is a structure designed to hold the electronics and power supply for the data acquisition and control system and other masses to balance the secondary mirror.

Other subsystems of the ASTREX test article include the Cold Gas Reaction Control system, the control moment gyroscopes, the Control and Data Acquisition Computer, and the cable follower.

The Cold Gas Reaction Control system, which consists of four pairs of 900 N (200 lbf) thrusters and six pairs of 36 N (8 lbf) thrusters mounted on the edges of the hexagonal primary structure, uses pressurized air to provide thrust. Pressurized air, with a maximum pressure of 480 psi, is supplied to the thrusters from two 30 gallon tanks inside the hub through a series of air hoses, ball valves and air filters.

The real-time Control and Data Acquisition Computer (CDAC) acquires data from the position encoder, the rate sensors and linear accelerometers on the ASTREX structure and commands the thrusters using MatrixX/Autocode software on a VAXstation 3100 workstation. The CDAC includes a VAXstation 3100 workstation as a front end, an INTEL 80386/Weitek 3167-based parallel processor unit, and an input/output unit having 32 input and 32 output channels for analog data as well as 64 bits of digital I/O. A high speed data link connects the CDAC input/output unit mounted on the tertiary structure with the parallel processor unit on the ground [9].

The actively-controlled, double-gimbal 3-axis cable follower is named for its main function of moving attached electrical, pneumatic, and communication cables to track the rigid-body movement of the ASTREX test article. This prevents these hanging cables from twisting or stretching, which would subsequently cause a resisting moment to the ASTREX structure movement.

Figure 2.2 shows the two inertial reference frames that are used to denote the current position and velocity of the ASTREX test article. The attitude of the airbearing is determined using three optical position encoders, mounted on the cable follower, which record the position counts with a sensitivity of 3 μrad. The cable follower computer converts the position counts to a 3-2-1 Euler angle set in the $\mathbf{n}_2$ reference frame and sends this data to the parallel processor unit through SCSI cabling. At this point, the 3-2-1 Euler angle set is converted to the corresponding Euler parameters in the $\mathbf{n}_2$ reference frame.

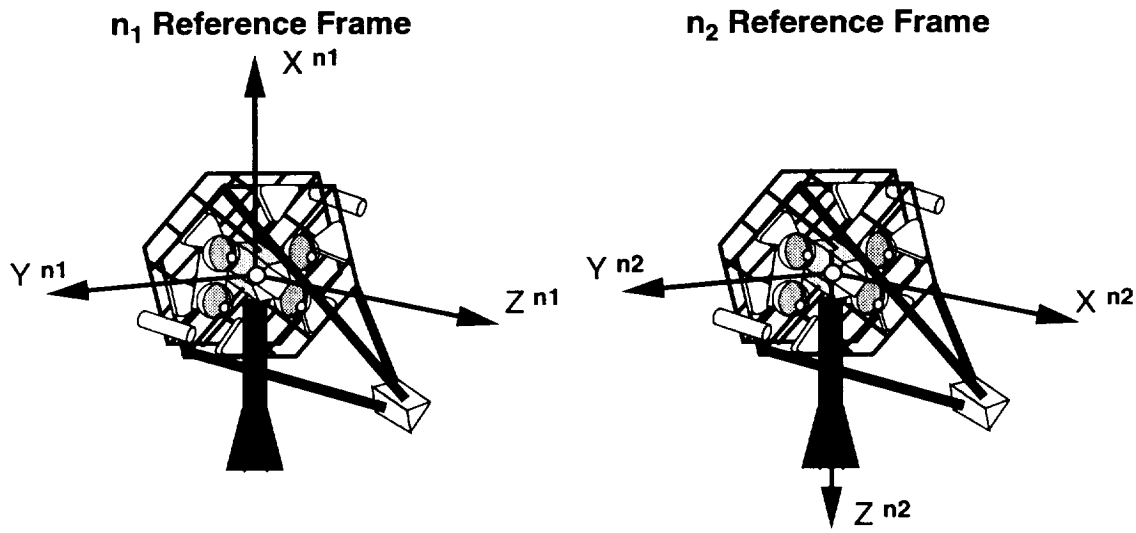

Figure 2.2. Inertial Reference Frames for the ASTREX Structure

Figure 2.3 displays the cable follower and the hemispherical ball of the airbearing. As the test article which is mounted on the hemispherical ball moves, the yaw position of the test article is followed by the motorized cable follower. Afterwards, its pitch and roll attitude are matched by the attached concentric rings which follow the movement of the ball; the order of these single-axis rotations is dependent on which of these concentric rings is outermost. Thus, Figure 2.3 demonstrates that the choice of the 3-2-1 Euler angle set for determining the current position of the air bearing is not arbitrary.

2.1. Airbearing to Body Reference Frame Coordinate Transformation

It is convenient to determine the Euler angles and the Euler parameters for the current body attitude with respect to the $\mathbf{n_1}$ reference frame. Based on the Euler angles from the cable follower computer, one can describe the current airbearing attitude in the inertial $\mathbf{n_2}$ reference frame:

$$\underline{\hat{a}} = C_{3-2-1}(\psi, \theta, \phi)\underline{\hat{n}}_2 \tag{2.1}$$

where the 3-2-1 Euler angle coordinate transformation matrix is defined as:

$$C_{3-2-1}(\theta_1, \theta_2, \theta_3) = D_1(\theta_3)D_2(\theta_2)D_3(\theta_1)$$

$$= \begin{bmatrix} \cos\theta_1\cos\theta_2 & \sin\theta_1\cos\theta_2 & -\sin\theta_2 \\ -\sin\theta_1\cos\theta_3 + \cos\theta_1\sin\theta_2\sin\theta_3 & \cos\theta_1\cos\theta_3 + \sin\theta_1\sin\theta_2\sin\theta_3 & \cos\theta_2\sin\theta_3 \\ \sin\theta_1\sin\theta_3 + \cos\theta_1\sin\theta_2\cos\theta_3 & -\cos\theta_1\sin\theta_3 + \sin\theta_1\sin\theta_2\cos\theta_3 & \cos\theta_2\cos\theta_3 \end{bmatrix} \tag{2.2}$$

The coordinate transformation matrix between two three-dimensional reference frames can be described with three single-axis rotations about three orthogonal axes. The following direction cosine matrices are used to perform these single axis rotations:

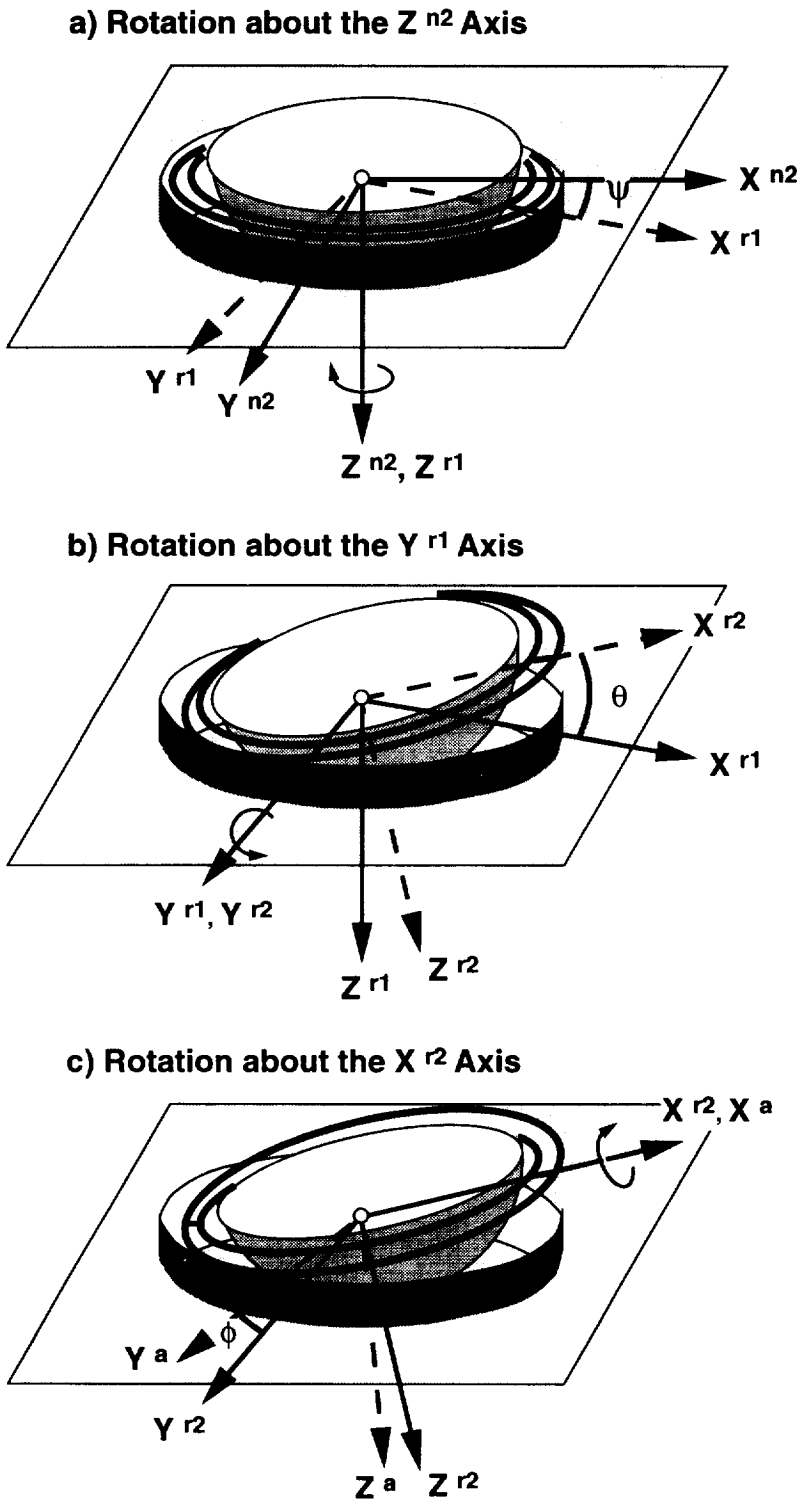

Figure 2.3. 3-2-1 Euler Angle Rotation Performed by the ASTREX Airbearing

$$D_1(\theta) = \begin{bmatrix} 1 & 0 & 0 \\ 0 & \cos\theta & \sin\theta \\ 0 & -\sin\theta & \cos\theta \end{bmatrix} \tag{2.3}$$

$$D_2(\theta) = \begin{bmatrix} \cos\theta & 0 & -\sin\theta \\ 0 & 1 & 0 \\ \sin\theta & 0 & \cos\theta \end{bmatrix} \tag{2.4}$$

$$D_3(\theta) = \begin{bmatrix} \cos\theta & \sin\theta & 0 \\ -\sin\theta & \cos\theta & 0 \\ 0 & 0 & 1 \end{bmatrix} \tag{2.5}$$

A single axis 90° pitch rotation is needed to transform vectors from the $\mathbf{n_1}$ to the $\mathbf{n_2}$ reference frame:

$$\underline{\hat{n}}_2 = D_2(-90°)\underline{\hat{n}}_1 \tag{2.6}$$

while the airbearing reference frame can be transformed to the body reference frame with a single-axis 60° pitch rotation:

$$\underline{\hat{b}} = D_2(60°)\underline{\hat{a}} \tag{2.7}$$

Thus, the following 1-2-3 Euler angle coordinate transformation in the $\mathbf{n_1}$ reference frame can be determined:

$$\begin{aligned} \underline{\hat{b}} &= C_{1-2-3}(\theta_1, \theta_2, \theta_3)\underline{\hat{n}}_1 \\ &= D_2(60°)C_{3-2-1}(\psi, \theta, \phi)D_2(-90°)\underline{\hat{n}}_1 \end{aligned} \tag{2.8}$$

where:

$$\begin{aligned} C_{1-2-3}(\theta_1, \theta_2, \theta_3) &= D_3(\theta_3)D_2(\theta_2)D_1(\theta_1) \\ &= \begin{bmatrix} \cos\theta_2\cos\theta_3 & \cos\theta_1\sin\theta_3 + \sin\theta_1\sin\theta_2\cos\theta_3 & \sin\theta_1\sin\theta_3 - \cos\theta_1\sin\theta_2\cos\theta_3 \\ -\cos\theta_2\sin\theta_3 & \cos\theta_1\cos\theta_3 + \sin\theta_1\sin\theta_2\sin\theta_3 & \sin\theta_1\cos\theta_3 - \cos\theta_1\sin\theta_2\cos\theta_3 \\ \sin\theta_2 & -\sin\theta_1\cos\theta_2 & \cos\theta_1\cos\theta_2 \end{bmatrix} \end{aligned} \tag{2.9}$$

The 1-2-3 Euler angles can be determined from this coordinate transformation matrix using inverse trigonometric relationships.

To determine the attitude in the body reference frame in a more computationally efficient algorithm, the coordinate transformation is performed using Euler parameters. The following Euler parameter set describes the 90° rotation about the y axis from the $\mathbf{n_2}$ to the $\mathbf{n_1}$ reference frame:

$$\underline{\beta}_{n1}^{\mathbf{n2}} = [0.7071 \quad 0 \quad 0.7071 \quad 0] \tag{2.10}$$

while the 60° rotation about the y axis to describe the body reference frame position from the airbearing reference frame position is given by:

$$\underline{\beta}_{b}^{\mathbf{a}} = [0.8660 \quad 0 \quad 0.5 \quad 0] \tag{2.11}$$

The Euler parameters can be transformed from the $\mathbf{n_2}$ to the $\mathbf{n_1}$ reference frame with the following equation:

$$\underline{\beta}_{a}^{\mathbf{n1}} = C^{\beta}_{\mathbf{n2}\rightarrow\mathbf{n1}}\left(\underline{\beta}_{n1}^{\mathbf{n2}}\right)\underline{\beta}_{a}^{\mathbf{n2}} \tag{2.12}$$

where

$$C^{\beta}_{\mathbf{n2}\rightarrow\mathbf{n1}}\left(\underline{\beta}_{n1}^{\mathbf{n2}}\right) = \begin{bmatrix} \beta_0 & \beta_1 & \beta_2 & \beta_3 \\ -\beta_1 & \beta_0 & \beta_3 & -\beta_2 \\ -\beta_2 & -\beta_3 & \beta_0 & \beta_1 \\ -\beta_3 & \beta_2 & -\beta_1 & \beta_0 \end{bmatrix} \tag{2.13}$$

To transform the Euler parameters from the airbearing reference frame to the body reference frame, the following coordinate transformation is used:

$$\underline{\beta}_{b}^{\mathbf{n1}} = C^{\beta}_{\mathbf{n1}\rightarrow\mathbf{n1}}\left(\underline{\beta}_{b}^{\mathbf{a}}\right)\underline{\beta}_{a}^{\mathbf{n1}} \tag{2.14}$$

where

$$C^{\beta}_{\mathbf{n1}\rightarrow\mathbf{n1}}\left(\underline{\beta}_{b}^{\mathbf{a}}\right) = \begin{bmatrix} \beta_0 & -\beta_1 & -\beta_2 & -\beta_3 \\ \beta_1 & \beta_0 & \beta_3 & -\beta_2 \\ \beta_2 & -\beta_3 & \beta_0 & \beta_1 \\ \beta_3 & \beta_2 & -\beta_1 & \beta_0 \end{bmatrix} \tag{2.15}$$

Thus, the Euler parameters which describe the body reference frame position in the inertial $\mathbf{n_1}$ reference frame can be directly obtained from the Euler parameters which describe the airbearing reference frame position in the inertial $\mathbf{n_2}$ reference frame with the following transformation:

$$\underline{\beta}_{b}^{\mathbf{n1}} = \begin{bmatrix} 0.9659 & 0.0 & 0.2588 & 0.0 \\ 0.0 & 0.2588 & 0.0 & -0.9659 \\ -0.2588 & 0.0 & 0.9659 & 0.0 \\ 0.0 & 0.9659 & 0.0 & 0.2588 \end{bmatrix} \underline{\beta}_{a}^{\mathbf{n2}} \tag{2.16}$$

2.2. Lowpass Digital Filter to Estimate Angular Velocity

The angular rate sensors for the ASTREX structure have a low frequency cut-off of 1 Hz. Precise attitude maneuvers cannot be accomplished with this bandwidth limitation. For example, the c.g. displacement creates oscillations at 0.05 Hz. Hence, a digital filter has been designed to estimate the current angular velocity from the Euler parameters.

The continuous-time differential equation for the Euler parameter time derivative is given by

$$\dot{\underline{\beta}} = \tfrac{1}{2} G(\underline{\beta})\underline{\omega} \tag{2.17}$$

where

$$G(\underline{\beta}) = \begin{bmatrix} -\beta_1 & -\beta_2 & -\beta_3 \\ \beta_0 & -\beta_3 & \beta_2 \\ \beta_3 & \beta_0 & -\beta_1 \\ -\beta_2 & \beta_1 & \beta_0 \end{bmatrix} \tag{2.18}$$

The above equation can be written in its inverted form as:

$$\underline{\omega}_k = 2G^T(\underline{\beta}_k)\dot{\underline{\beta}}_k \tag{2.19}$$

The Euler parameter time derivative can be estimated with a digital filter which differentiates the Euler parameter measurements. A second order filter of the form

$$G_1(s) = \frac{ab\,\mathrm{s}}{(\mathrm{s}+a)(\mathrm{s}+b)} \tag{2.20}$$

was selected for this purpose to maintain a reasonable computational burden. The poles of the filter were selected to provide an adequate derivative estimation at low frequencies and attenuate high frequency noise. Transforming this filter to the z-domain space using a bilinear transformation which keeps the poles at the same location, one obtains:

$$G_1(z) = k\,G_2(z) = \frac{k\,(\mathrm{z}-1)(\mathrm{z}+1)}{\left(\mathrm{z}-e^{-aT}\right)\left(\mathrm{z}-e^{-bT}\right)} \tag{2.21}$$

where T is the sampling interval. The multiple k is used to constrain the filter magnitude from the Bode plot to 1 at a frequency of 1 rad/sec.

$$k = \frac{1}{\mathrm{Magn}\left(G_1(z,\omega=1)\right)} \tag{2.22}$$

The highest frequency from the open-loop Euler parameters would occur during the thrust impulse at the beginning or the end of the bang-off-bang maneuver. This signal has an approximate frequency of 0.25 Hz (1.57 rad/sec). A good differentiator should have the following characteristics on the Bode plot:

1. A low frequency slope of 20 dB/decade
2. A phase angle of 90°

Hence, the design criteria are to keep the phase change from 90° as small as possible at low frequencies. The allowable phase lag due to the filter is determined based on experimental results.

Table 2.1 shows the design trade-offs in choosing the poles for a second-order filter which will perform both differentiation of low frequencies and attenuation of high frequencies. Using Filter 1 from this table for a final position regulation experiment of the ASTREX test article resulted in unacceptable performance with terminal oscillations. When this same experiment was repeated using Filter 3 from Table 2.1, this oscillation disappeared. The phase change in Filter 1 was presumed to be too high. Although Filter 3 did work, its output was too noisy. Thus, a phase change design criteria was set at -3.0 deg. for a frequency of 1 rad/sec; the noise amplification at 100 rad/sec was minimized, when possible, while meeting this design criteria. Filter 5 was the final choice for the second-order filter which could be designed under these constraints. If this filter is implemented in hardware or the host computer for this control system is updated in the future, a better alternative would be to design a higher order filter.

2.3. Determination of the Control Influence Matrix

The thrust from the thrusters can be varied by controlling the voltages with the CDAC. To control a three-axis rotation of the ASTREX structure, the thrusters must generate a moment about the pivot point to reach the desired final attitude. To calculate this time-varying moment, a non-dimensional control vector $\underline{u}$ is defined which is related to the moment generated by the thrusters and the voltages which regulate the thruster's force.

Table 2.1. Digital Filter Design Trade-Offs to Achieve Low Frequency Differentiation and High Frequency Attenuation

Filter #	Continuous Time Poles (Hz)	Digital Filter	Phase Change at ω=1 rad/sec (deg.)	Magn. at ω=100 rad/sec
1	1.0, 1.0	$\frac{0.0790\left(z^2-1\right)}{z^2-1.9504z+0.9510}$	-16.26	0.40
2	1.64, 1.64	$\frac{0.2057\left(z^2-1\right)}{z^2-1.9192z+0.9209}$	-9.98	1.05
3	10.0, 10.0	$\frac{6.1750\left(z^2-1\right)}{z^2-1.5555z+0.6049}$	-1.65	27.93
4	10.0, 50.0	$\frac{19.8755\left(z^2-1\right)}{z^2-1.0624z+0.2214}$	-1.01	50.00
5	3.5, 12.0	$\frac{2.7436\left(z^2-1\right)}{z^2-1.6554z+0.6774}$	-3.03	12.77

The moment generated by the thrusters is defined in the body reference frame:

$$\underline{M}^{\mathbf{b}}_{Thr} = \sum_{i=1}^{nf} \left(\underline{r}^{\mathbf{b}} \times \underline{F}^{\mathbf{b}} \right)_i = \sum_{i=1}^{nf} \tilde{r}_i \underline{F}_i \tag{2.23}$$

where the bold superscript **b** denotes the body reference frame. *nf* is the total number of thruster sets. $\tilde{r}$ is the cross product matrix of each thruster set position:

$$\tilde{r} = \begin{bmatrix} 0 & -r_3 & r_2 \\ r_3 & 0 & -r_1 \\ -r_2 & r_1 & 0 \end{bmatrix} \tag{2.24}$$

$\underline{F}$ is the force vector for each thruster set. A thruster set is defined as a device which can produce positive and negative thrust from its mounted position; thus, the two 200 lb. uniaxial thrusters that are mounted at the same location and generate thrust in opposing directions form a single thruster set. The moment is related to the non-dimensional control vector $\underline{u}$ with the control influence matrix B:

$$\underline{M}^{\mathbf{b}}_{Thr} = B\underline{u} \tag{2.25}$$

The components of the control influence matrix are determined from the partial derivative of the moment vector which is taken with respect to the control vector.

$$B = \frac{\partial \underline{M}^{\mathbf{b}}_{Thr}}{\partial \underline{u}} = \frac{\partial}{\partial \underline{u}} \left\{ \sum_{i=1}^{nf} \tilde{r}_i \underline{F}_i \right\} \tag{2.26}$$

The control influence matrix relationship is more flexible for systems with various actuator configurations if the matrix B is the product of two independent matrices: a matrix which defines the location and thrust of each thruster set and a second matrix $T_{U_{comb}}$ which will define the desired control-moment relationship for three-axis rotational control.

$$B = \left[\tilde{r}_1 \underline{F}_1 \quad \tilde{r}_2 \underline{F}_2 \quad \cdots \quad \tilde{r}_{nf} \underline{F}_{nf} \right] T_{U_{comb}} \tag{2.27}$$

The thrusters fire along the $\pm z^{\mathbf{n}}$ axis when the ASTREX structure is in its initial rest position. Therefore, the maximum force generated by each thruster set will be determined by multiplying each thruster set's saturation thrust $\underline{T}_{Sat}$ by its positive voltage thrust direction in the absolute reference frame $T^{\mathbf{n}}_{+V\,Dir}$ and then transfer this force matrix to the body reference frame by rotating -30° about the $y^{\mathbf{n}}$ axis using the direction cosine matrix.

$$F^{\mathbf{b}} = \left[\underline{F}^{\mathbf{b}}_1 \quad \underline{F}^{\mathbf{b}}_2 \quad \cdots \quad \underline{F}^{\mathbf{b}}_{nf} \right] = k_{N/lb.}\, D_2(-30°)\, T^{\mathbf{n}}_{+V\,Dir} diag\left(\underline{T}_{Sat} \right) \tag{2.28}$$

where the conversion factor to Newtons from pounds is given by

$$k_{N/lb.} = 4.4484 \text{ N/lb.} \tag{2.29}$$

and the direction cosine matrix D_2 about the $y^{\mathbf{n}}$ axis is defined by eqn. (2.3). The bold superscript **b** denotes the components in the body reference frame, while the bold superscript **n** denotes the components in the inertial reference frame.

The control influence matrix B is defined by the:

1. Thruster Set Location relative to the Pivot Point
2. Saturation Thrust of each Thruster Set
3. Positive Voltage Thrust Direction of each Thruster Set
4. Control-Moment Relationship for each Thruster Set

Figure 2.4 shows the positive voltage thrust direction for the 8 lb. and 200 lb. thruster sets. From this diagram, the following two matrices, which define the saturation thrust for each thruster set and the corresponding positive voltage thrust direction in the absolute reference frame, are constructed.

$$\underline{T}_{Sat} = [8 \quad 8 \quad 8 \quad 8 \quad 8 \quad 8 \quad 200 \quad 200 \quad 200 \quad 200] \tag{2.30}$$

$$T^{n}_{+V\,Dir} = \begin{bmatrix} 0 & 0 & 0 & 0 & 0 & 0 & 0 & 0 & 0 & 0 \\ 0 & 0 & 0 & 0 & 1 & 1 & 0 & 0 & 0 & 0 \\ 1 & 1 & 1 & 1 & 0 & 0 & 1 & 1 & 1 & 1 \end{bmatrix} \tag{2.31}$$

Each thruster set column in the saturation thrust matrix and the positive voltage thrust direction matrix is ordered by the corresponding thruster manufacture number given in Figure 2.4. The rows in the positive voltage thrust direction matrix denote whether each thruster set is firing in the x^n, y^n, or z^n axis. The sign of each value in the positive voltage thrust direction matrix is defined by whether the thruster fires in the positive or negative absolute reference frame axis direction. Table 2.2 summarizes the location of each thruster set, the saturation thrust of each thruster set and its positive voltage thrust direction.

Table 2.2. Individual Thruster Set Location, Saturation Thrust, and Positive Voltage Thrust Direction

Thruster Manufacture #	Node #	X^b (m)	Y^b (m)	Z^b (m)	Thrust Sat. & +V Dir. (lb)
1	327	-1.36581	-2.7116	-0.30839	+8 z^n
2	325	1.33419	-2.7116	-0.30839	+8 z^n
3	321	1.33419	2.7116	-0.30839	+8 z^n
4	323	-1.36581	2.7116	-0.30839	+8 z^n
5	427	-2.84230	0.0	-0.10658	+8 y^n
6	437	2.81068	0.0	-0.10658	+8 y^n
7 (1-2)	324	-1.36581	2.5465	-0.30839	+200 z^n
8 (3-4)	322	1.33419	2.5465	-0.30839	+200 z^n
9 (5-6)	328	-1.36581	-2.5465	-0.30839	+200 z^n
10 (7-8)	326	1.33419	-2.5465	-0.30839	+200 z^n

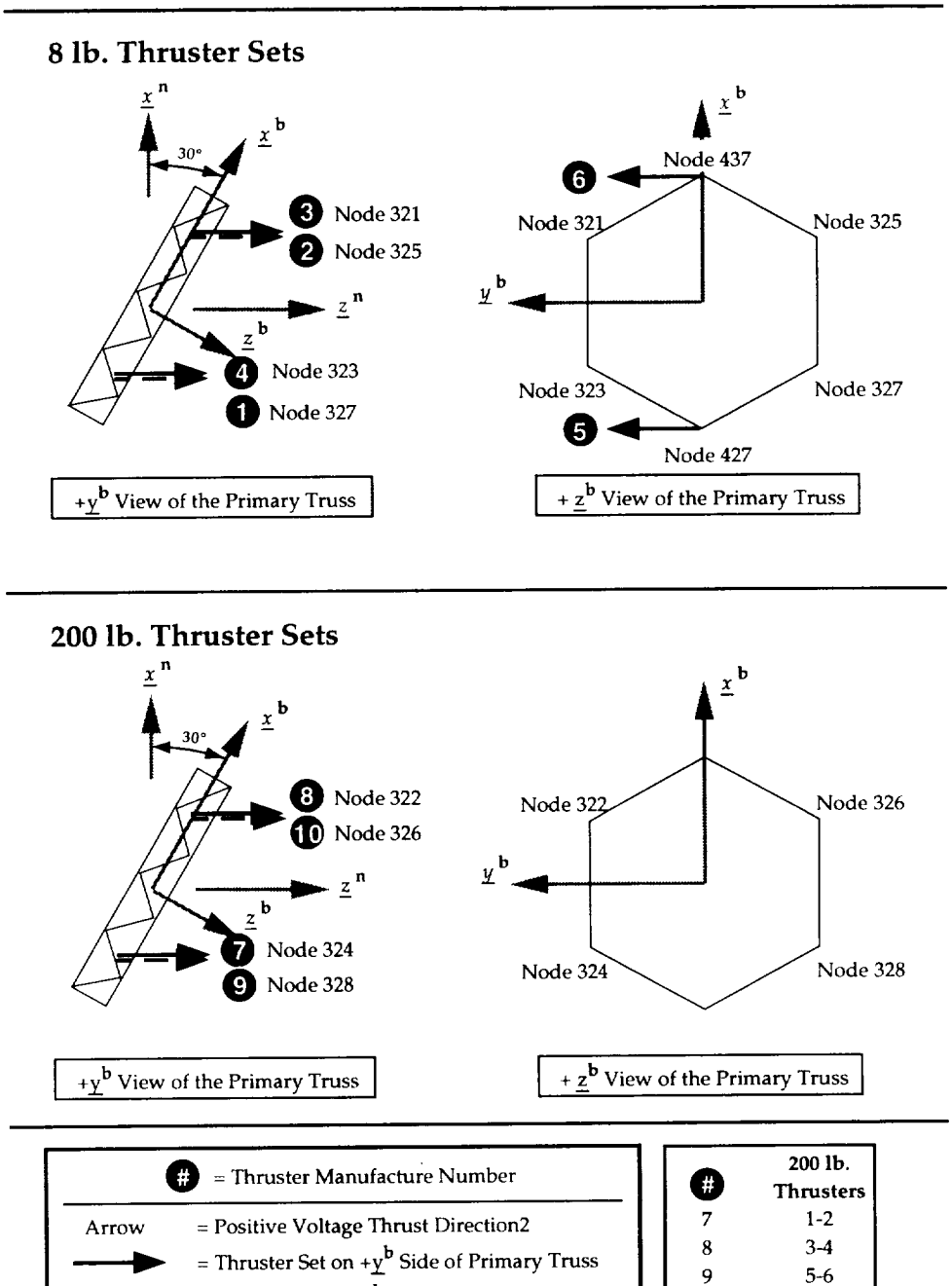

Figure 2.4. Positive Voltage Thrust Direction for Each Thruster Set

2.4. Thruster Control-Moment Relationship

For the dynamical system to be controllable, three independent moments about three primary axes must be generated. Since the ASTREX test article is mounted on a fixed pivot point, the available thrusters must be combined such that pure moments are generated about the pivot point. In addition, since the optimization method for determining the minimum-time control requires that saturation limits be placed on the controls, the control saturation limits must be directly related to the physical saturation limits of each thruster. Each control will be limited to a range of [-1, +1], which reflects the maximum thrust in opposing directions for each individual thruster it commands.

A thruster combination set is a group of thruster sets which fire simultaneously for a given control u_i to produce a moment about a fixed control axis. To produce a pure rotation without translation, the thruster combination set usually consists of thruster sets with similar saturation thrusts. If a control axis is coincident with a body axis, the thruster combination set allows a single control to apply a pure moment about that body axis. If all control axes are coincident with the body axes, the control influence matrix is diagonal. However, the thruster set locations on the ASTREX structure cannot be combined to form this diagonal control influence matrix.

A thruster configuration is a set of three thruster combination sets which provides three-axis rotational control; each configuration will provide a positive moment about the control axis if the control u is positive. A positive moment is one which adheres to the right hand rule about the control axis. Different thruster configurations are denoted by the saturation thrust for the thruster sets in each of the three thruster combination sets.

Figure 2.4 shows that thruster sets 5 and 6 are located at equal distances from the pivot point and only generate thrust in the $\pm y^b$ directions. Thus, a thruster combination set including thruster sets 5 and 6 can control the roll motion of ASTREX. The remaining thruster sets on the ASTREX test article provide thrust in both the $\pm x^b$ directions and the $\pm z^b$ directions. Although a single control could provide a pure moment about the y^b axis, a single control cannot provide a pure moment about the x^b axis. Therefore, a diagonal control influence matrix is impossible with the given thruster set locations. Fortunately, both the four remaining 8 lb. thruster sets and the four remaining 200 lb. thruster sets form the corners of a rectangle with the pivot point in the rectangle's center. This symmetry is utilized in generating a moment about a fixed axis.

The 200-200-8 configuration or the 8-8-8 configuration controls the yaw and pitch axes using the four corresponding 200 lb. thruster sets or 8 lb. thruster sets respectively. Both the 200 lb. and 8

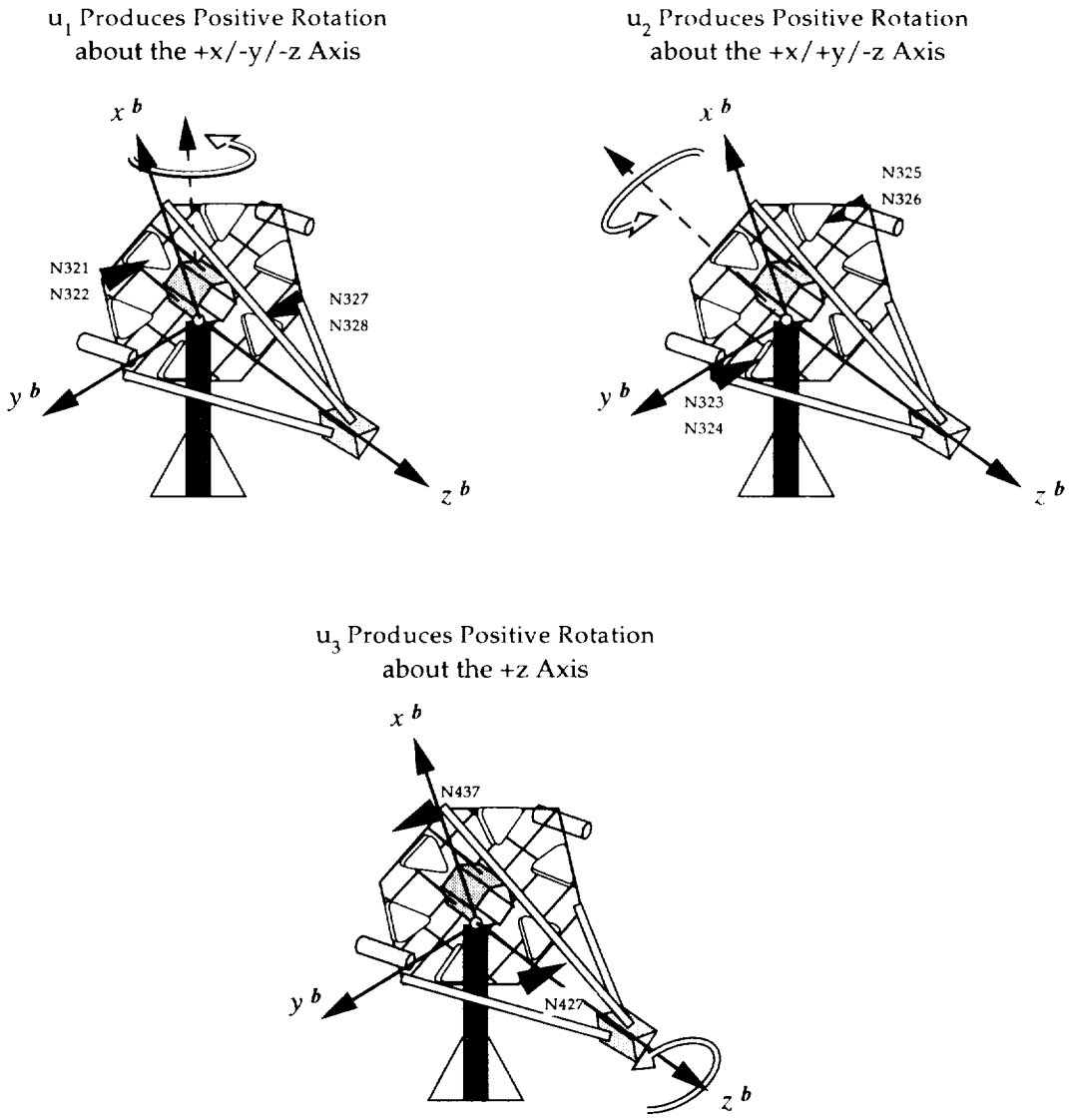

Figure 2.5. Three-Axis Rotational Control Using the 200-200-8 Thruster Configuration or the 8-8-8 Thruster Configurations

lb. thruster sets are placed in a similar rectangular arrangement about the pivot point. To maintain a direct relationship between the thruster sets and a single control, the four thruster sets are divided into two thruster sets connected to u_1 and two thruster sets connected to the u_2. The thruster sets on the diagonal corners of each rectangle are used to form a thruster combination set. Figure 2.5 displays the control axis for each thruster combination set in these configurations. These thruster combination sets produce a moment about the +x/-y/-z axis and the +x/+y/-z axis; however, these two axes are not orthogonal. Thus, the u_1 and the u_2 controls generate yaw, pitch, and roll moments. Although these two thruster combination sets do provide somewhat symmetrical moments, knowledge of the control history does not provide an intuitive understanding of the resulting maneuver. The thruster configuration defines the control-moment

relationship in the $T_{U_{comb}}$ matrix:

$$T_{U_{8-8-8}} = \begin{bmatrix} -1 & 0 & 0 \\ 0 & -1 & 0 \\ 1 & 0 & 0 \\ 0 & 1 & 0 \\ 0 & 0 & -1 \\ 0 & 0 & 1 \\ \hline \multicolumn{3}{c}{\underset{4\times 3}{0}} \end{bmatrix} \tag{2.32}$$

$$T_{U_{200-200-8}} = \begin{bmatrix} \multicolumn{3}{c}{\underset{4\times 3}{0}} \\ \hline 0 & 0 & -1 \\ 0 & 0 & 1 \\ 0 & 1 & 0 \\ 1 & 0 & 0 \\ -1 & 0 & 0 \\ 0 & -1 & 0 \end{bmatrix} \tag{2.33}$$

Table 2.3 summarizes each thruster set's control-moment relationship for the three thruster configurations. The thrust is determined from the control vector using the following equation:

$$\underline{Thr} = diag\left(\underline{T}_{Sat}\right) T_{U_{comb}} \underline{u} \tag{2.34}$$

The relationship between the thrust and the control voltage $\underline{V}$ is given by a similar equation:

$$\underline{Thr} = diag\left(\underline{k}_{lb./V}\right)\underline{V} \tag{2.35}$$

Table 2.3. Control-Moment Relationship for each Thruster Configuration

		Thruster Configuration	
Thruster Manufacture #	Node #	8-8-8 Thruster Configuration	200-200-8 Thruster Configuration
1	327	$-u_1$	--
2	325	$-u_2$	--
3	321	u_1	--
4	323	u_2	--
5	427	$-u_3$	$-u_3$
6	437	u_3	u_3
7 (1-2)	324	--	u_2
8 (3-4)	322	--	u_1
9 (5-6)	328	--	$-u_1$
10 (7-8)	326	--	$-u_2$

Table 2.4. Relationships Between Voltage, Thrust, and Air Pressure for each Thruster Set

Thruster Manufacture #	Node #	$k_{lb./V}$	$k_{V/lb.}$	$k_{psi./V}$	$k_{V./psi}$
1	327	1.193	0.8382	25.063	0.00398
2	325	1.116	0.8960	26.882	0.00372
3	321	1.255	0.7968	24.146	0.00414
4	323	1.164	0.8591	25.773	0.00388
5	427	1.107	0.9033	27.109	0.00369
6	437	1.163	0.8598	25.795	0.003876
7 (1-2)	324	25.0	0.04	2.0	0.5
8 (3-4)	322	25.0	0.04	2.0	0.5
9 (5-6)	328	25.0	0.04	2.0	0.5
10 (7-8)	326	25.0	0.04	2.0	0.5

where the $\underline{k}_{lb./V}$ gain vector defines the pounds per volt ratio for each thruster set. Setting the thrust equations equal to each other, we can form the relationship between the control vector and the voltage vector:

$$\underline{V} = diag\left(\underline{k}_{V/lb.}\right) diag\left(\underline{T}_{Sat}\right) T_{U_{comb}} \underline{u} \tag{2.36}$$

Table 2.4 shows the voltage gains for the ASTREX test article.

2.5. Equations of Motion for the ASTREX Test Article

Although the ASTREX test article is a large, fairly rigid space structure, the truss structures composed of interconnected graphite-epoxy tubes are inherently flexible. Due to the displaced center of gravity position, the lowest mode for the test article is approximately 0.05 Hz. A finite-element model of the combined ASTREX test article/pedestal system is used to determine the flexible modes for this structure up to 50 Hz [9]. The bending of the pedestal causes a mode at about 3.4 Hz, while the lowest test article bending mode is located at 10 Hz. It is evident that the control-structure interaction can take place at the low end of the spectrum (.05 Hz) to the first structural mode frequency (3.4 Hz) and beyond. The high frequency interaction is attenuated using smooth control profiles, while the low frequency interaction is actively controlled. For this reason, the rigid body dynamics model will be sufficient to design the open-loop and feedback controls.

Since the pivot point is fixed for the ASTREX test article, only the rotational equations of motion are considered. The rotational equations of motion are defined using the Euler parameter time

derivative and the angular acceleration. For an intuitive understanding of the motion, the Euler parameters are converted to the 1-2-3 Euler angle set to visualize the maneuvers.

The Euler parameter time derivative is given by (Alternate form of eqn. (2.17)):

$$\dot{\underline{\beta}} = \frac{1}{2} G(\underline{\omega})\underline{\beta} \tag{2.37}$$

where the Euler parameters $\underline{\beta}$ are in the inertial reference frame and the matrix $G(\underline{\omega})$ is given by:

$$G(\underline{\omega}) = \begin{bmatrix} 0 & -\omega_1 & -\omega_2 & -\omega_3 \\ \omega_1 & 0 & \omega_3 & -\omega_2 \\ \omega_2 & -\omega_3 & 0 & \omega_1 \\ \omega_3 & \omega_2 & -\omega_1 & 0 \end{bmatrix} \tag{2.38}$$

where $\underline{\omega}$ represents the angular velocity vector in the body reference frame. The angular velocity time derivative is given by:

$$\dot{\underline{\omega}} = I^{-1}\left(\underline{M}_{ext} - \tilde{\omega} I \underline{\omega}\right) \tag{2.39}$$

I designates the inertia matrix in the body reference frame and $\tilde{\omega}$ represents the angular velocity cross-product matrix.

$$\tilde{\omega} = \begin{bmatrix} 0 & -\omega_3 & \omega_2 \\ \omega_3 & 0 & -\omega_1 \\ -\omega_2 & \omega_1 & 0 \end{bmatrix} \tag{2.40}$$

The external moments on the body are generated only by the thrusters:

$$\underline{M}_{ext} = \underline{r}_{Thr} \times \underline{F}_{Thr} = B\underline{u} \tag{2.41}$$

where B is the control influence matrix, $\underline{r}_{Thr}$ is the distance from the pivot point to each thruster location, and $\underline{F}_{Thr}$ is the force produced by each individual thruster. The $\underline{u}$ vector in the thruster moment is a non-dimensional control vector with values in the range of [-1,+1].

The limited volume of pressurized air available for each maneuver places an inequality constraint on this control problem. To verify that this fuel constraint is satisfied, the fuel mass flow rate is integrated over the entire maneuver time to determine the total fuel depletion. The fuel volume flow rate is a function of the combined absolute value thrust components for each axis:

$$\dot{V}_{fuel} = -2\, k_{fuel/Thr} \sum_{i=1}^{3} \left| T_{Comb\,Sat,i}\, u_i \right| \tag{2.42}$$

$\underline{T}_{Comb\,Sat}$ defines the saturation thrust (lbs. force) for each thruster in a given thruster combination, while $k_{fuel/Thr}$ is the conversion factor from lbs. force to ft^3 per sec provided by the manufacturer.

3.0. OPEN-LOOP & CLOSED-LOOP CONTROL THEORY FOR NEAR MINIMUM-TIME MANEUVERS

The basic control problem is to move the ASTREX test article from the initial rest position to a final rest position in minimum time. Since a finite fuel supply is available for this maneuver, the minimum-time control is not the unconstrained minimum-time control predicted by calculus of variations theory.[10,11] In fact, the available fuel is so limited that the optimal control is closer to the bang-off-bang type for all but the smallest maneuvers.[12] Torque smoothing is incorporated into the open-loop control design to prevent the discontinuous jumps in the input control from exciting the unmodeled high frequency structural modes. The optimized near minimum-time open-loop control must be augmented with feedback control to achieve fine pointing due to the presence of unmodeled dynamics, imprecise initial conditions and parametric uncertainty. Thus, a globally asymptotically stable Lyapunov control was designed to converge on the final attitude. Although the Lyapunov closed-loop control is not designed to minimize fuel consumption, closed-loop simulations can be used to predict the amount of fuel which will be required. The engineer must determine the amount of fuel for the open-loop optimization based on the anticipated closed-loop fuel requirements.

3.1. Near Minimum-Time Open-Loop Control

It is well known from optimal control theory that time-optimal controls are bang-bang, if singular intervals are not present. If the fuel constraint is active and singular intervals are still not present, the time-optimal controls are bang-off-bang: the control will fully saturate, shut off (during this time, the structure will coast), and then fully saturate in the opposite direction.[10,11] Since the mathematical model of the test article might include many "real-world" effects not encountered in classical textbook problems, parameter optimization was used to determine the open-loop control profiles rather than the rigorous two-point boundary value problem.

Since the control profiles must be smooth to prevent excitation of the high frequency modes, a multiplier function is used:

$$m(\eta) = \eta^2(3-2\eta), \quad \eta \in [0,1] \tag{3.1}$$

In this equation, η defines whether the control is off, saturated, or undergoing a smooth transition between two control levels. To define η, the researcher must specify the non-dimensional rise time τ_{rise}, the non-dimensional time that the saturated control occurs τ_{sat}, the initial control magnitude u_1 and the final control magnitude after the rise time u_2.

$$\eta = \begin{cases} 0, \text{ No Control} \\ u_{sat}, \text{ Saturated Control} \\ u_2 + (u_2 - u_1)\dfrac{\tau - \tau_{sat}}{\tau_{rise}}, \text{ Saturation Ahead, } \tau \in [\tau_{sat} - \tau_{rise}, \tau_{sat}] \\ u_1 + (u_2 - u_1)\dfrac{\tau - \tau_{sat}}{\tau_{rise}}, \text{ Saturation Behind, } \tau \in [\tau_{sat}, \tau_{sat} + \tau_{rise}] \end{cases} \tag{3.2}$$

The bang-off-bang control can be parameterized using:

- Individual Saturation Control, p_{sat}
- Smoothing Multiplier Rise Time, p_{rise}

These parameters are optimized for the performance index and the given boundary conditions using the Sequential Quadratic Programming (SQP) algorithm, which solves nonlinear programming problems. The SQP problem is constructed by first defining the performance index, the equality and inequality constraints, and the inclusive upper and lower parameter limits. The minimum-time SQP problem using the bang-off-bang parameters is formulated as: [8]

$$\text{Minimize } J = \tfrac{1}{2} p_0{}^2 \text{ subject to:}$$

$$\begin{cases} \underline{x}_f - \underline{x}_{bc}(1) = 0 \\ V_{fuel\,Available} - \int_0^1 \dot{V}_{fuel}\, d\tau \geq 0 \\ 1^* \leq p_0 \leq 60^* \\ -1 \leq \underline{p}_{sat} \leq 1 \\ 0.05^* \leq \underline{p}_{rise} \leq 0.25 \end{cases} \tag{3.3}$$

$\underline{x_f}$ defines the desired final boundary condition states, while the integrated states are given by:

$$\underline{x}_{bc}{}^T = [\beta_1 \quad \beta_2 \quad \beta_3 \quad \omega_1 \quad \omega_2 \quad \omega_3] \tag{3.4}$$

The asterisks in the above equation denotes numbers which are arbitrarily chosen parameter constraints. A commercial SQP algorithm such as the one included in the IMSL Math Libraries can optimize the parameters with little programming effort by the researcher.

3.2. Lyapunov Control for Final Position Regulation

For rest-to-rest maneuvers, the desired final angular velocity is zero. The equilibrium state can be defined where the error vectors between the current state and the final state go to zero.

$$\begin{Bmatrix} \underline{e}_\beta \\ \underline{e}_\omega \end{Bmatrix} = \begin{Bmatrix} \underline{\beta} - \underline{\beta}_f \\ \underline{\omega} \end{Bmatrix} = \underline{0} \tag{3.5}$$

The state equations for these functions include the Euler parameter error time derivative and the angular velocity error time derivative:

$$\begin{Bmatrix} \dot{\underline{e}}_\beta \\ \dot{\underline{e}}_\omega \end{Bmatrix} = \begin{Bmatrix} \dot{\underline{\beta}} - \dot{\underline{\beta}}_f \\ \dot{\underline{\omega}} \end{Bmatrix} = \begin{Bmatrix} \frac{1}{2} G(\beta)\underline{\omega} \\ I^{-1}(B\underline{u} - \tilde{\omega} I \underline{\omega} + \underline{M}_{dist}) \end{Bmatrix} \tag{3.6}$$

where I is the inertia matrix. The disturbance moment $\underline{M}_{dist}$ is neglected for this derivation. However, this closed-loop control law derivation is valid in the presence of the moments from additional dynamics determined from the system identification.

The following positive definite Lyapunov function is chosen to prove that this nonlinear system can be asymptotically stable with the proper choice of the control torque:[3,4]

$$V(\underline{e}_\beta, \underline{e}_\omega) = \tfrac{1}{2}\underline{e}_\beta{}^T P_{11}\underline{e}_\beta + \tfrac{1}{2}\underline{e}_\omega{}^T P_{22}\underline{e}_\omega \tag{3.7}$$

where P_{11} and P_{22} are constant, symmetric positive definite gain matrices. By choosing the control as:

$$\underline{u} = B^{-1}\left[-IP_{22}{}^{-1}\left(\tfrac{1}{2}G^T(\underline{\beta})P_{11}\underline{e}_\beta + Q\underline{\omega}\right) + \tilde{\omega}I\underline{\omega} - \underline{M}_{dist}\right] \tag{3.8}$$

the Lyapunov function time derivative is negative semidefinite:

$$\dot{V}(\underline{e}_\beta, \underline{e}_\omega) = -\underline{e}_\omega{}^T Q\underline{e}_\omega \tag{3.9}$$

where Q is a symmetric positive definite gain matrix. By looking at the third time derivative of the Lyapunov function[13], it can be easily shown that the Lyapunov function will only go to zero when the error function of the Euler parameters goes to zero. Therefore, this final position regulation control will be asymptotically stable in the large.

3.3. Lyapunov Control for Tracking a Reference Trajectory

Since the near-minimum time control for rotational maneuvers of the ASTREX structure is calculated offline, the trajectory defined by this control should be near-optimal, despite small modeling errors. Therefore, we would like the ASTREX structure to track this trajectory for the entire maneuver. The equilibrium state can be defined where the error vectors between the current state and the reference trajectory state go to zero.[3,7]

$$\begin{Bmatrix}\underline{e}_\beta \\ \underline{e}_\omega\end{Bmatrix} = \begin{Bmatrix}\underline{\beta} - \underline{\beta}_{ref} \\ \underline{\omega} - \underline{\omega}_{ref}\end{Bmatrix} = \underline{0} \tag{3.10}$$

The state equations for these functions include the Euler parameter error time derivative and the angular velocity error time derivative:

$$\begin{Bmatrix}\dot{\underline{e}}_\beta \\ \dot{\underline{e}}_\omega\end{Bmatrix} = \begin{Bmatrix}\dot{\underline{\beta}} - \dot{\underline{\beta}}_{ref} \\ \dot{\underline{\omega}} - \dot{\underline{\omega}}_{ref}\end{Bmatrix} = \begin{Bmatrix}\tfrac{1}{2}\left(G(\beta)\underline{\omega} - G\left(\beta_{ref}\right)\underline{\omega}_{ref}\right) \\ I^{-1}\left[B\left(\underline{u} - \underline{u}_{ref}\right) - \left(\tilde{\omega}I\underline{\omega} - \tilde{\omega}_{ref}I\underline{\omega}_{ref}\right) + \left(\underline{M}_{dist} - \underline{M}_{dist\,ref}\right)\right]\end{Bmatrix} \tag{3.11}$$

Again, the disturbance moment $\underline{M}_{dist}$ is neglected for the remainder of this derivation. The following positive definite Lyapunov function is chosen to prove that this nonlinear system can be asymptotically stable with the proper choice of the control torque:

$$V(\underline{e}_\beta, \underline{e}_\omega) = \tfrac{1}{2}\underline{e}_\beta{}^T P_{11}\underline{e}_\beta + \tfrac{1}{2}\underline{e}_\omega{}^T P_{22}\underline{e}_\omega \tag{3.12}$$

where P_{11} and P_{22} are constant, symmetric positive definite gain matrices. By choosing the control as:

$$\underline{u} = \underline{u}_{ref} + B^{-1}\left[-IP_{22}{}^{-1}\left(\frac{\rho}{2}G^T\left(\underline{\beta}_{ref}\right)\underline{\beta} + Q\underline{e}_\omega\right) + \left(\tilde{\omega}I\underline{\omega} - \tilde{\omega}_{ref}I\underline{\omega}_{ref}\right) - \left(\underline{M}_{dist} - \underline{M}_{dist\,ref}\right)\right] \quad (3.13)$$

where ρ is a positive scalar which has replaced the positive gain matrix P_{11}, the Lyapunov function time derivative will be negative semidefinite:

$$\dot{V}(\underline{e}_\beta, \underline{e}_\omega) = -\underline{e}_\omega{}^T Q\underline{e}_\omega \quad (3.14)$$

where Q is a symmetric positive definite gain matrix. By looking at the third time derivative of the Lyapunov function, it can be easily shown that the Lyapunov function will only go to zero when the error function of the Euler parameters goes to zero. Therefore, this reference trajectory tracking control will be asymptotically stable in the large.

3.4. Gain Matrix Selection from a Damped System Analogy

If we substitute eqn. (3.13) into eqn. (3.11), the following second order system is constructed:

$$\dot{\underline{e}}_\omega + P_{22}{}^{-1}Q\underline{e}_\omega + \frac{\rho}{2}P_{22}{}^{-1}G^T\left(\underline{\beta}_{ref}\right)\underline{\beta} = \underline{0} \quad (3.15)$$

Furthermore, it is true that the reduced Euler parameter vector, which describes the current Euler parameter in the reference frame with the reference Euler parameter as an origin, is given by:

$$\tilde{\underline{\beta}}^{\mathbf{ref}} = G^T\left(\underline{\beta}_{ref}\right)\underline{\beta}^{\mathbf{n1}} \quad (3.16)$$

Assuming small errors, the difference between the current position and the reference maneuver position can be approximated in Euler angles as:

$$\tilde{\underline{\beta}}^{\mathbf{ref}} \approx \frac{1}{2}\left(\underline{\theta} - \underline{\theta}_{ref}\right) = \frac{1}{2}\underline{e}_\theta = \frac{1}{2}\int_0^t \underline{e}_\omega\, dt \quad (3.17)$$

Substituting this term into eqn. (3.15), the tracking error second order system is described by:

$$\dot{\underline{e}}_\omega + P_{22}{}^{-1}Q\underline{e}_\omega + \frac{\rho}{4}P_{22}{}^{-1}\underline{e}_\theta = \underline{0} \quad (3.18)$$

To determine the scalar gain and the gain matrices in an intuitive manner, this system is related to a damped second order system, where ω_n is the natural frequency and ξ is the damping coefficient. Therefore, the scalar gain and the gain matrices are defined as:

$$\rho = 4\omega_n{}^2 \quad (3.19)$$

$$P_{22} = I_{33} \quad (3.20)$$

$$Q = 2\xi\omega_n I_{33} \quad (3.21)$$

where I_{33} is the 3 x 3 identity matrix. Using these relationships, an engineer must only choose the damping coefficient and the natural frequency for this system to meet the desired performance requirements. In addition, the Lyapunov function and its time derivative reduce to:

$$V(t, \underline{e}_\beta, \underline{e}_\omega) = 2\omega_n{}^2\underline{e}_\beta{}^T\underline{e}_\beta + \frac{1}{2}\underline{e}_\omega{}^T\underline{e}_\omega \quad (3.22)$$

$$\dot{V} = -2\xi\omega_n\underline{e}_\omega{}^T\underline{e}_\omega \quad (3.23)$$

Using these gains, the final position regulator control is given by:

$$\underline{u} = -2B^{-1}\left[I\left(\omega_n{}^2G^T\left(\underline{\beta}_f\right)\underline{\beta} + \xi\omega_n\underline{\omega}\right) + \underline{M}_{dist}\right] \quad (3.24)$$

while the tracking control is given by:

$$\underline{u} = \underline{u}_{ref} + B^{-1}\left[-2I\left(\omega_n{}^2 G^T\left(\underline{\beta}_{ref}\right)\underline{\beta} + \xi\omega_n \underline{e}_\omega\right) + \tilde{\omega} I\,\underline{\omega} - \tilde{\omega}_{ref} I\,\underline{\omega}_{ref} + \underline{M}_{dist} - \underline{M}_{dist\,ref}\right] \tag{3.25}$$

3.5. Convergence Rate Estimate from the Lyapunov Function

The convergence rate of the Lyapunov function control can be examined by expressing the Lyapunov function time derivative as a function of the Lyapunov function itself. Assume that the Lyapunov function and its time derivative can be expressed in the following form:

$$V = \underline{x}^T P \underline{x} \tag{3.26}$$

$$\dot{V} = -\underline{x}^T Q \underline{x} \tag{3.27}$$

where P is a positive definite gain matrix and Q is a positive semidefinite gain matrix which satisfies the asymptotic stability of the Lyapunov function. It is well known from matrix theory that:

$$\begin{aligned} \lambda_{\min}(P)\underline{x}^T\underline{x} \le \underline{x}^T P \underline{x} \le \lambda_{\max}(P)\underline{x}^T\underline{x} \\ \lambda_{\min}(Q)\underline{x}^T\underline{x} \le \underline{x}^T Q \underline{x} \le \lambda_{\max}(Q)\underline{x}^T\underline{x} \end{aligned} \tag{3.28}$$

Thus, the following inequality relationship between the Lyapunov function and its time derivative is formed:

$$\underline{x}^T Q \underline{x} \ge \lambda_{\min}(Q)\underline{x}^T\underline{x} \ge \frac{\lambda_{\min}(Q)}{\lambda_{\max}(P)}\underline{x}^T P \underline{x} \ge \frac{\lambda_{\min}(Q)}{\lambda_{\max}(P)} V \tag{3.29}$$

This process can be repeated to determine the lower bound for the Lyapunov function time derivative:

$$\frac{\lambda_{\max}(Q)}{\lambda_{\min}(P)} V \le \dot{V} \le \frac{\lambda_{\min}(Q)}{\lambda_{\max}(P)} V \tag{3.30}$$

This can be solved to determine the bounds for the Lyapunov function:

$$e^{-\frac{\lambda_{\max}(Q)}{\lambda_{\min}(P)}(t-t_0)} V(t_0) \le V(t) \le e^{-\frac{\lambda_{\min}(Q)}{\lambda_{\max}(P)}(t-t_0)} V(t_0) \tag{3.31}$$

Similarly, the upper and lower bound for the L_2-norm of the state vector can be determined similarly:

$$\frac{V(t_0)}{\lambda_{\max}(P)} e^{-\frac{\lambda_{\max}(Q)}{\lambda_{\min}(P)}(t-t_0)} \le \left\|\underline{x}(t)\right\|_2{}^2 \le \frac{V(t_0)}{\lambda_{\min}(P)} e^{-\frac{\lambda_{\min}(Q)}{\lambda_{\max}(P)}(t-t_0)} \tag{3.32}$$

$$\left[\frac{V(t_0)}{\lambda_{\max}(P)}\right]^{\frac{1}{2}} e^{-\frac{\lambda_{\max}(Q)}{2\lambda_{\min}(P)}(t-t_0)} \le \left\|\underline{x}(t)\right\|_2 \le \left[\frac{V(t_0)}{\lambda_{\min}(P)}\right]^{\frac{1}{2}} e^{-\frac{\lambda_{\min}(Q)}{2\lambda_{\max}(P)}(t-t_0)} \tag{3.33}$$

If Q is a positive semidefinite matrix, the state norm will only have an exponential lower bound:

$$\left[\frac{V(t_0)}{\lambda_{\max}(P)}\right]^{\frac{1}{2}} e^{-\frac{\lambda_{\max}(Q)}{2\lambda_{\min}(P)}(t-t_0)} \le \left\|\underline{x}(t)\right\|_2 \le \left[\frac{V(t_0)}{\lambda_{\min}(P)}\right]^{\frac{1}{2}} \tag{3.34}$$

Since the final position regulator and the tracking controls have the same structure for their respective Lyapunov functions and Lyapunov function time derivatives, the convergence rates of these controls can be determined simultaneously. These convergence rates are only applicable in the maneuver when the closed loop control is the only control applied. Therefore, the time t_0 normally refers to the final time for the open-loop maneuver. In both cases, the Lyapunov function time derivative is only a function of the angular velocity errors:

$$V(\underline{e}_\beta, \underline{e}_\omega) = 2\omega_n{}^2 \underline{e}_\beta{}^T \underline{e}_\beta + \tfrac{1}{2} \underline{e}_\omega{}^T \underline{e}_\omega \tag{3.35}$$

$$\dot{V}(\underline{e}_\beta, \underline{e}_\omega) = -2\xi\omega_n \underline{e}_\omega{}^T \underline{e}_\omega \tag{3.36}$$

Thus, the state error norm is bounded by:

$$\begin{aligned} \left[2V(t_0)\right]^{\frac{1}{2}} e^{-\frac{\xi}{2\omega_n}(t-t_0)} \le \left\| \begin{Bmatrix} \underline{e}_\beta \\ \underline{e}_\omega \end{Bmatrix} \right\|_2 \le \left[\frac{1}{2\omega_n{}^2} V(t_0)\right]^{\frac{1}{2}} \text{ if } \omega_n \in \left(0, \tfrac{1}{2}\right] \\ \left[\frac{1}{2\omega_n{}^2} V(t_0)\right]^{\frac{1}{2}} e^{-2\xi\omega_n(t-t_0)} \le \left\| \begin{Bmatrix} \underline{e}_\beta \\ \underline{e}_\omega \end{Bmatrix} \right\|_2 \le \left[2V(t_0)\right]^{\frac{1}{2}} \text{ if } \omega_n \in \left(\tfrac{1}{2}, \infty\right) \end{aligned} \tag{3.37}$$

Thus, to increase the convergence rate,

$$\text{Maximize} \begin{cases} \frac{\xi}{2\omega_n} \text{ if } \omega_n \in \left(0, \frac{1}{2}\right] \\ 2\xi\omega_n \text{ if } \omega_n \in \left(\frac{1}{2}, \infty\right) \end{cases} \tag{3.38}$$

The actual choice of these parameters must be determined by the control magnitude and the convergence properties of the states. By setting a tolerance on the state norm, one can estimate the least time that this closed-loop control takes to move the state norm below this criterion from the above lower bound.

4.0. SYSTEM IDENTIFICATION

The control for a near minimum-time 60° yaw maneuver was optimized using a sequential quadratic programming (SQP) algorithm to determine the bang-off-bang maneuver parameters for a 100 psi pressure loss constraint. The ASTREX control interface could only command 50 lb. of thrust for the 200 lb. thrusters and 5 lb. of thrust for the 8 lb. thrusters. Since the closed-loop control would need additional thrust to perform fine pointing, the open-loop control was optimized under a maximum saturation constraint of 20 lb. for the 200 lb. thrusters and 2 lb. for the 8 lb. thrusters. In April 1993, this experiment was performed using the ASTREX test article. Figure 4.1 shows the simulated states and thrust for this maneuver, while Figure 4.2 show the experimental states and thrust.

From these experimental results, the following problems were determined:

- The small displacement of the center of gravity (c.g.) from the pivot point causes lightly damped oscillations in the pitch and the roll Euler angles.
- The actual thruster force is much less than the simulated thruster force.
- The relationship between the actual and simulated thruster force changes during the acceleration and deceleration phases of the maneuver.
- Thruster dynamics change differently for the 8 lb. and 200 lb. thrusters as the air tank pressure decreases. The thrust is clipped when the 8 lb. thrusters fire with the air tank pressure below 150 psi or when the 200 lb. thrusters fire with the air tank pressure below 30 psi.
- Pressure leakage reduces the available fuel for the maneuver. The most significant pressure loss (~200 psi) occurred initially when the ball valves first open to allow compressed air in the thruster chambers and connecting tubes.
- Unexpected thruster firings from stray command voltages caused large amplitude maneuvers of the test article, which consequently aborted many tests.

Testing continued from April 1993 to November 1993 to identify the reasons for these problems and to determine a mathematical model which would accurately describe the effect on the dynamical system. Appendix A contains a listing of the tests which were performed during this project. Table A-1 gives a brief description of the reference maneuver for each test, while Table A-2 lists the experimental attitude maneuvers and their unique characteristics.

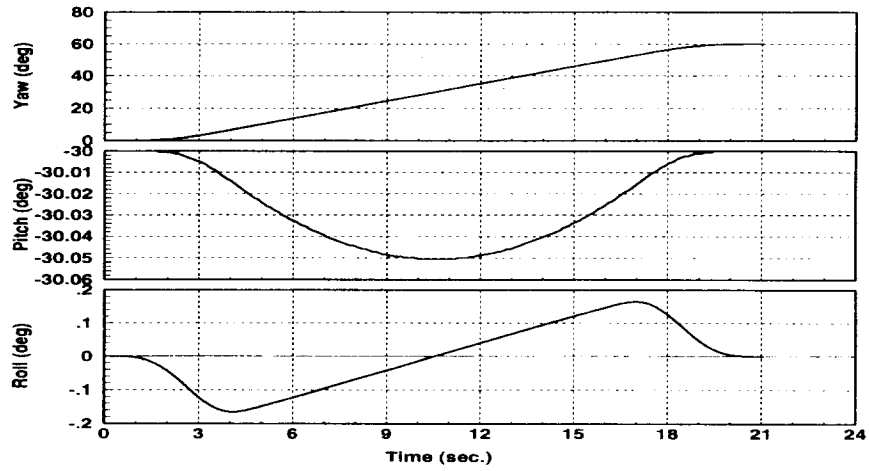

(a) Euler Angles during Maneuver

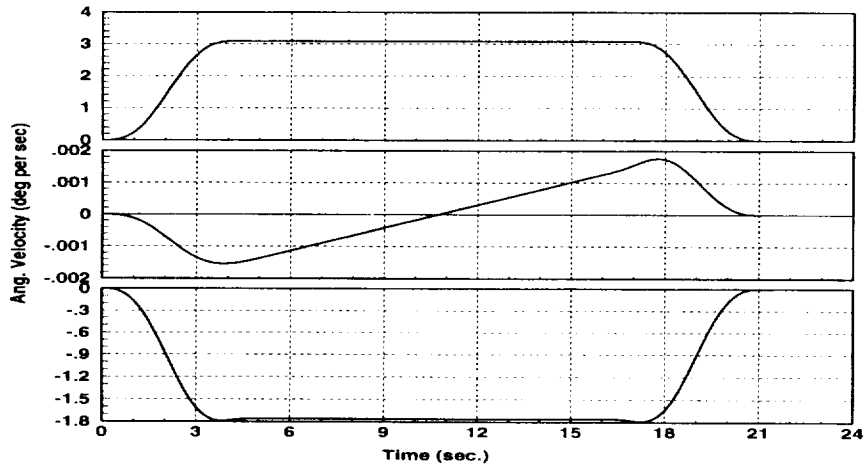

(b) Angular Velocities during Maneuver

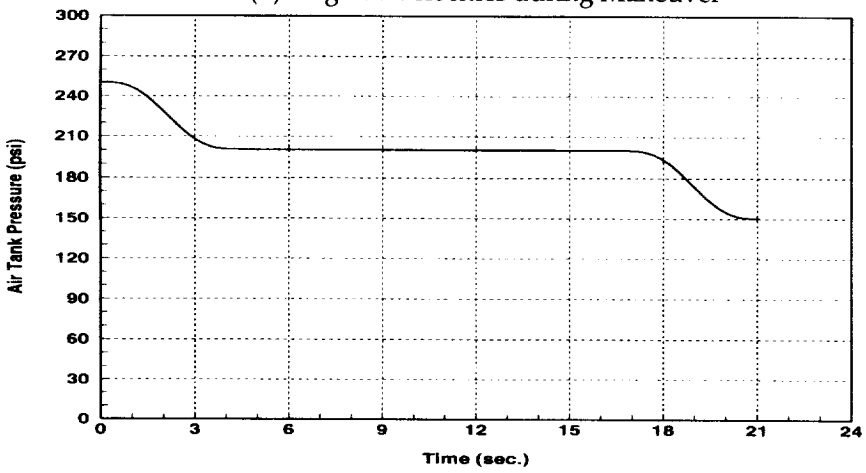

(c) Air Tank Pressure during Maneuver

Figure 4.1. States and Thrust for the 60° Yaw Maneuver Simulation (test13_sim_ref)

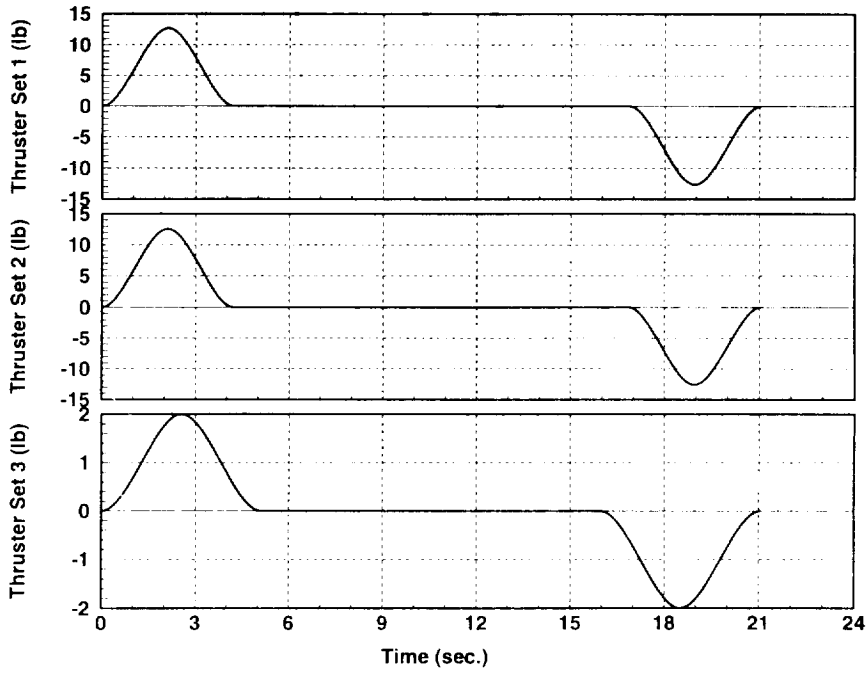

(d) Thrust during Maneuver

Figure 4.1. States and Thrust for the 60° Yaw Maneuver Simulation (test13_sim_ref) (cont'd)

4.1. Equilibrium Position for the ASTREX Test Article

The c.g. for the test article is not exactly coincident with the pivot point. In the $\mathbf{n_1}$ reference frame, the moment on the test article due to the force caused by this displaced c.g. is determined by:

$$\underline{M}_{cg}^{\mathbf{n1}} = \underline{r}_{cg}^{\mathbf{n1}} \times \underline{F}^{\mathbf{n1}} = \underline{r}_{cg}^{\mathbf{n1}} \times \begin{Bmatrix} -mg \\ 0 \\ 0 \end{Bmatrix} \tag{4.1}$$

The equilibrium position for the test article is reached when the moment due to the displaced c.g. goes to zero. Obviously, this occurs when the effective center of gravity position is directly below the pivot point. Thus, only one parameter is needed to position the center of gravity along this vertical path. An initial displacement from the equilibrium position causes a low frequency oscillation about the $\mathbf{n_1}$ -frame pitch and roll axes. In the body reference frame, the moment due to the displaced c.g. position are attitude-dependent.

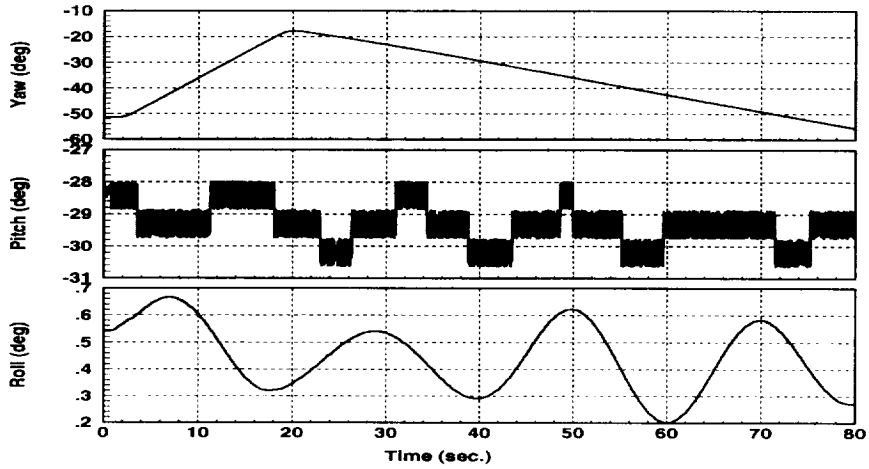

(a) Euler Angles during Maneuver

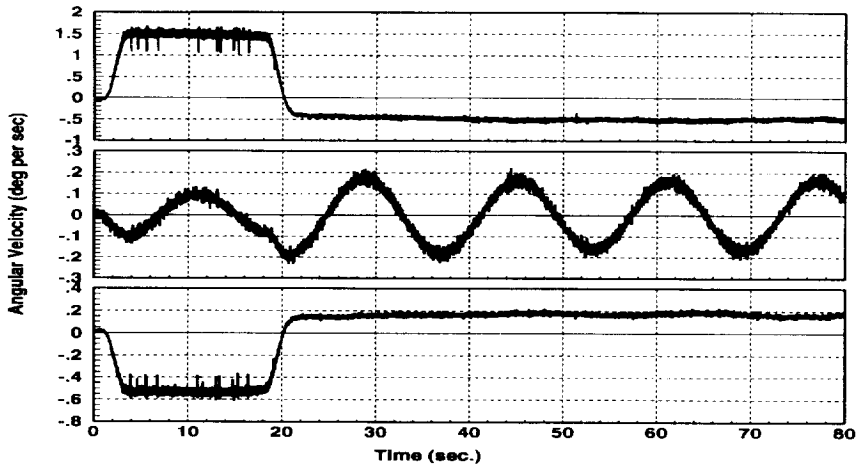

(b) Angular Velocities during Maneuver

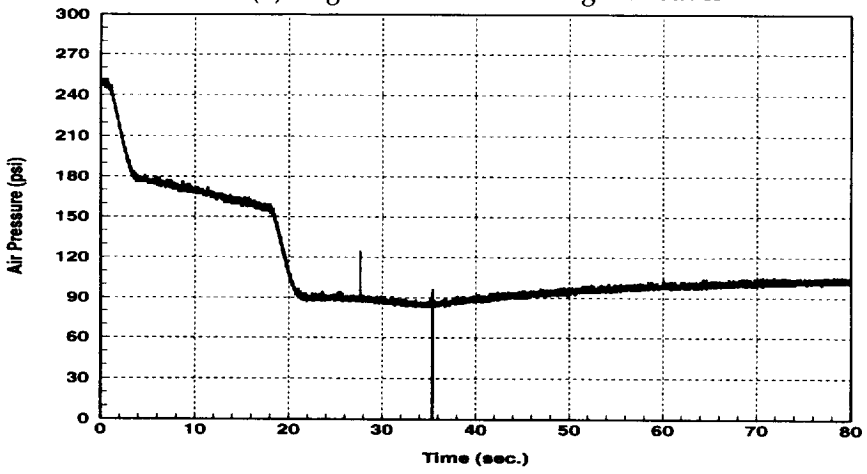

(c) Air Tank Pressure during Maneuver

Figure 4.2. States and Thrust for the 60° Yaw Maneuver Experiment (test13_exp1)

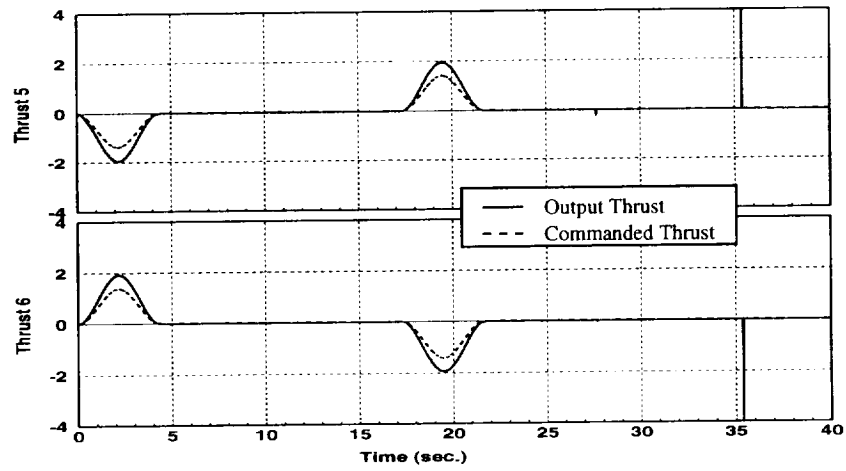

(d) Commanded & Actual Thrust during Maneuver (8 lbf Thrusters)

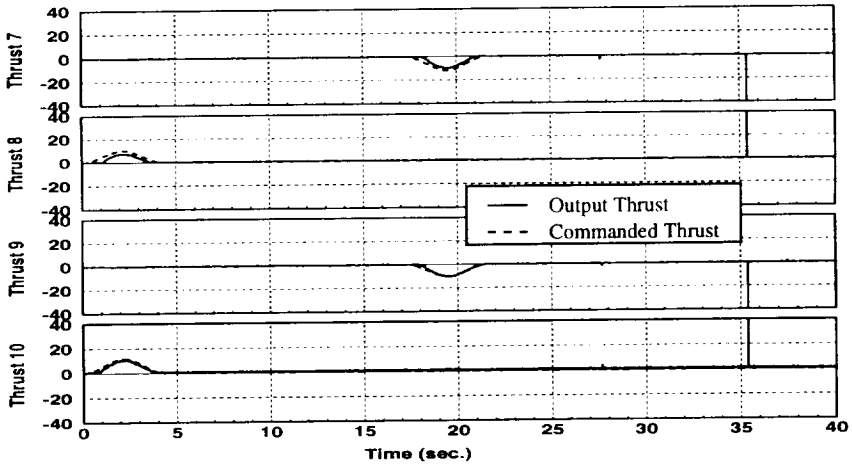

(e) Commanded & Actual Thrust during Maneuver (200 lbf Thrusters)

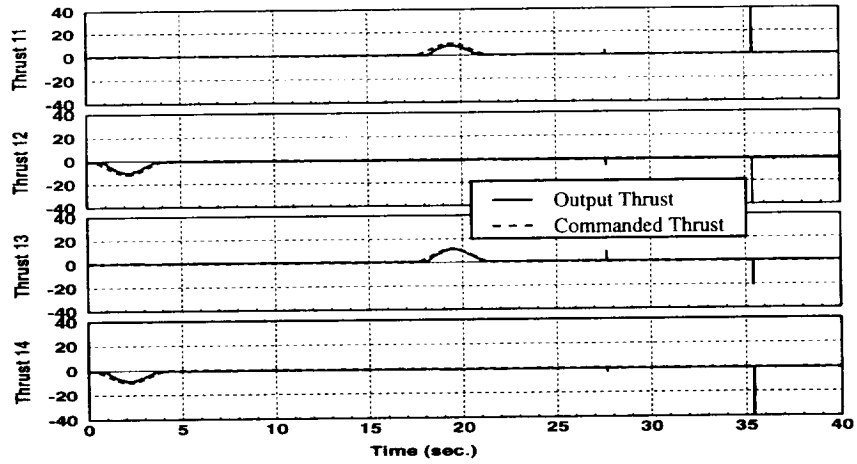

(f) Commanded & Actual Thrust during Maneuver (200 lbf Thrusters)

Figure 4.2. States and Thrust for the 60° Yaw Maneuver Experiment (test13_exp1) (cont'd)

$$\underline{M}_{cg}^{\mathbf{b}} = \underline{r}_{cg}^{\mathbf{b}} \times \underline{F}^{\mathbf{b}} = \underline{r}_{cg}^{\mathbf{b}} \times C_{1-2-3}\left(\theta_1, \theta_2, \theta_3\right)\begin{Bmatrix} -mg \\ 0 \\ 0 \end{Bmatrix} \tag{4.2}$$

However, the radius vector from the pivot point to the c.g. will not vary in this reference frame.

Although the finite element model of the combined ASTREX test article / pedestal system defines the total mass of the test article and the location of its c.g. position, this information did not correspond to the known rest position for the ASTREX structure. Therefore, experimental tests were needed to determine the effective c.g. position. Free oscillation tests were performed on the ASTREX test article with initial displacements about each of the body axes. The pitch and the roll components of the resultant equilibrium position are unique due to the displacement of the c.g. from the pivot point. Figure 4.3 (a) shows the Euler angles from the free oscillation tests with an initial pitch displacement, while Figure 4.3 (b) shows the Euler angles from the free oscillation tests with an initial roll displacement. The roll oscillation frequency is approximately 0.0455 Hz, while the pitch oscillation frequency is approximately 0.0588 Hz. From these tests, the Euler angle equilibrium position was estimated to be:

$$\underline{\theta}_{eq}^{\mathbf{n1}} = \begin{bmatrix} -- & -29.2 & 0.23 \end{bmatrix} \text{deg.} \tag{4.3}$$

A system identification on the free oscillation data determined the value of the c.g. vertical position parameter x_{cg} by minimizing the error norm between the simulation and the experimental measurements. The test article mass was assumed to be equal to the mass approximation from the finite element model.

$$m = 4004.8 \text{ kg} \tag{4.4}$$

Thus, the c. g. position in the body reference frame is determined by:

$$\underline{r}_{cg}^{\mathbf{b}} = C_{1-2-3}\left(\theta_{eq1}, \theta_{eq2}, \theta_{eq3}\right)\begin{Bmatrix} x_{cg}^{\mathbf{n1}} \\ 0 \\ 0 \end{Bmatrix} \tag{4.5}$$

The current c.g. position has been determined as:

$$\underline{r}_{cg}^{\mathbf{b}} = \begin{bmatrix} -0.02147 & 0.00086 & 0.01200 \end{bmatrix} \text{m} \tag{4.6}$$

Table A-3 details the equilibrium tests that have currently been performed on the ASTREX test article.

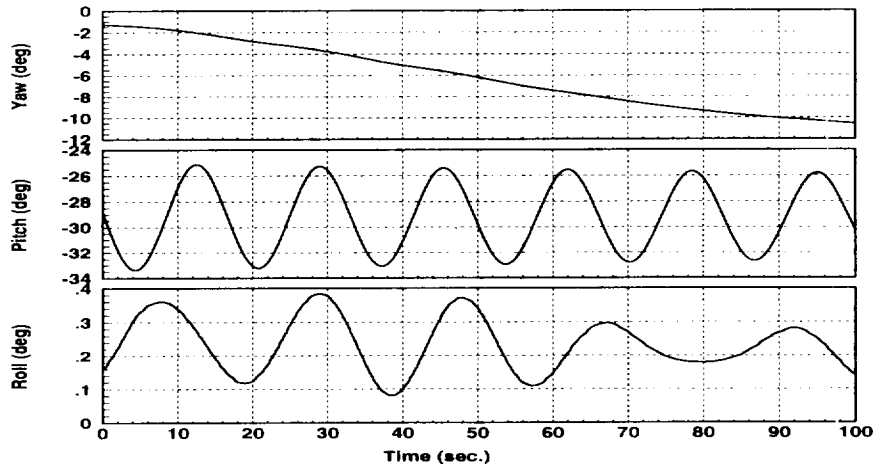

(a) Initial Pitch Displacement (eq_test1_exp1)

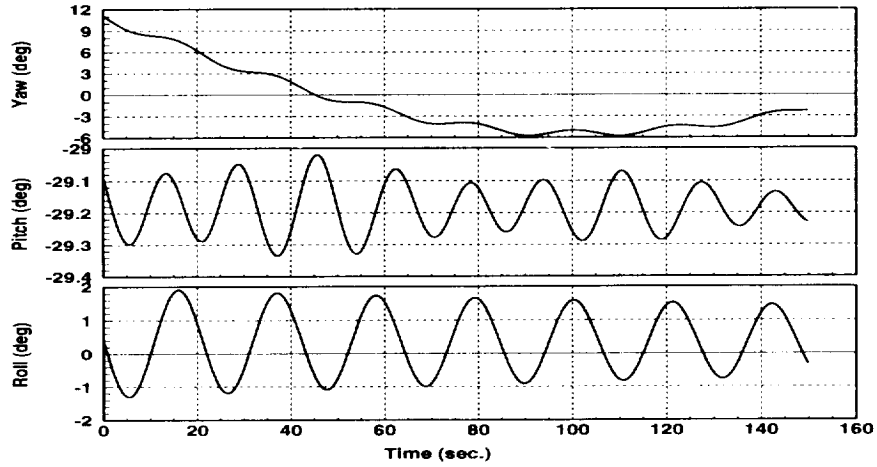

(b) Initial Roll Displacement (eq_test1_exp2)

Figure 4.3. Free Oscillation Tests

4.2. Revised State Equations for the ASTREX Structure

The external moment in the angular acceleration can be revised to show the effect of the displaced c.g. and the acceleration/deceleration relationship between the simulated and actual thrust:

$$\underline{M}_{ext} = diag\left(\underline{k}_{Thr\,Eff}\right)B\underline{u} - mg\tilde{r}_{cg}\begin{Bmatrix} C_{11} \\ C_{21} \\ C_{31} \end{Bmatrix} \tag{4.7}$$

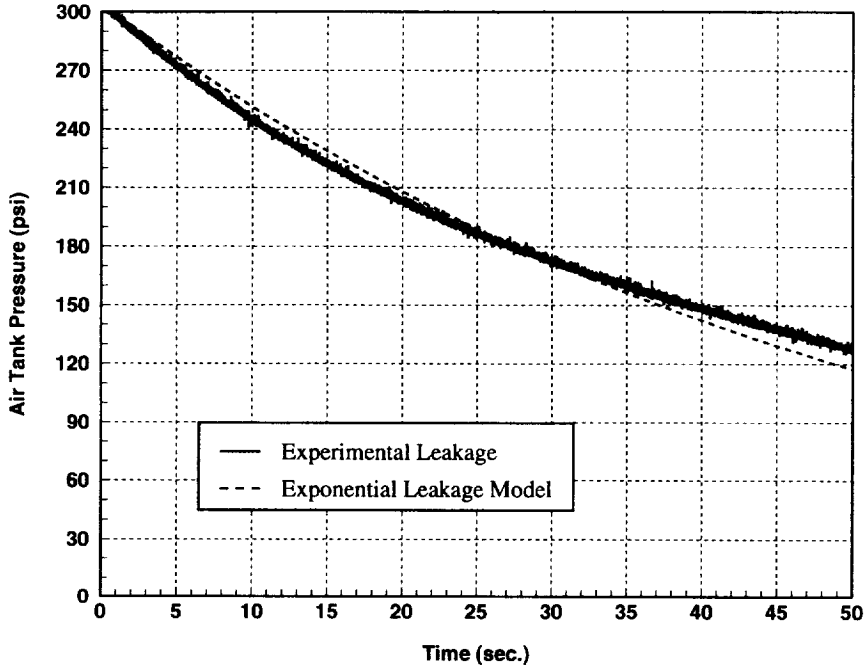

Figure 4.4. Air Tank Pressure for Leakage Test (plk_test_exp1)

where

$$\underline{k}_{Thr\,Eff} = \begin{cases} [0.85 \quad 0.85 \quad 0.85]^T, \text{ Accel.} \\ [0.97 \quad 0.97 \quad 0.97]^T, \text{ Decel.} \end{cases} \tag{4.8}$$

These thruster efficiency gains are not determined directly, but by minimizing the overall error between the simulated and actual states for a maneuver. The physical meaning of this gain vector could be a static friction component, a thruster dynamics change due to the air tank pressure, or an inaccurate estimate of the moment of inertia matrix. To account for the thrust difference between the simulated and actual thrust, the control influence matrix is redefined as:

$$B = \frac{\partial}{\partial \underline{u}}\left(\underline{r} \times diag\left(\underline{k}_{Actual\,Thr}\right)\underline{F}\right) \tag{4.9}$$

where

$$\underline{k}_{Actual\,Thr} = [1.26 \quad 1.26 \quad 1.26 \quad 1.26 \quad 1.26 \quad 1.27 \quad 1.00 \quad 1.06 \quad 0.99 \quad 1.02] \tag{4.10}$$

The actual thrust gain vector is determined by dividing the peak actual thrust norm by the peak simulated thrust norm for each individual thruster set.

To investigate the pressure leakage, an experiment was performed by recording the air tank pressure while the ASTREX test article was at rest. The dashed line in Figure 4.4 is an exponential estimate of this pressure loss given by the following equation:

$$p(t) = p_0 \; e^{-c\,p_0 t} \tag{4.11}$$

where c is the pressure leakage constant. This pressure leakage model is included in the revised air volume flow rate:

$$\dot{V}_{fuel} = -2k_{fuel/Thr} \sum_{i=1}^{3} \left| k_{Comb\,Sat,i}\, u_i \right| - c\, p_0 V_{fuel} \tag{4.12}$$

c is the leakage constant which determines the volume flow rate due to the current volume of air at atmospheric pressure in the air tank remaining to be discharged.

$$c = 6.26e-5 \text{ sec}^{-1} \tag{4.13}$$

The maximum saturation thrust for each thruster combination is given by:

$$k_{Comb\,Sat} = \begin{bmatrix} 200 & 200 & 8 \end{bmatrix}^T \text{lb.} \tag{4.14}$$

while the conversion between thrust and the air volume flow rate is given by:

$$k_{fuel/Thr} = 0.3081 \; \frac{\text{ft}^3}{\text{lb-sec}} \tag{4.15}$$

Table A-4 presents a brief description of this pressure leakage test.

Currently, the ASTREX moment of inertia matrix in the body reference frame has been determined from a finite element model to be:

$$I = \begin{bmatrix} 18{,}941. & -25.0 & -243.0 \\ -25.0 & 11{,}804. & 25.0 \\ -243.0 & 25.0 & 14{,}188. \end{bmatrix} kg-m^2 \tag{4.16}$$

The control influence matrix is given by:

$$B = \begin{bmatrix} 4022. & 3963. & 0.62 \\ -2144. & 2104. & 0. \\ -2322. & -2288. & 254.48 \end{bmatrix} N-m \tag{4.17}$$

In current experiments, the 200 lb. thrusters are constrained to only use 30 lb. for the open-loop control, while the 8 lb. thrusters can use 3 lb. With the increased air volume flow rate due to the pressure leakage, the yaw maneuver was constrained to only 30°. Computationally, it was determined that even this small maneuver would not be possible without using more fuel. Thus, the desired pressure loss for the optimized open-loop maneuver was reset to 140 psi. Since the initial experimental air pressure in Figure 4.2 (c) was approximately 250 psi, this increase in the fuel used for the open-loop control still leaves enough fuel to perform fine pointing.

Figure 4.5 shows the simulated states and thrust for the revised dynamics for a 30° maneuver,

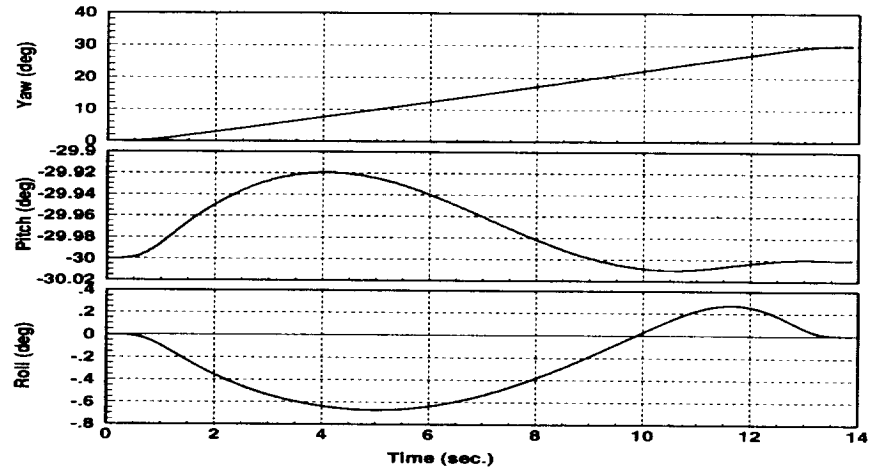

(a) Euler Angles during Maneuver

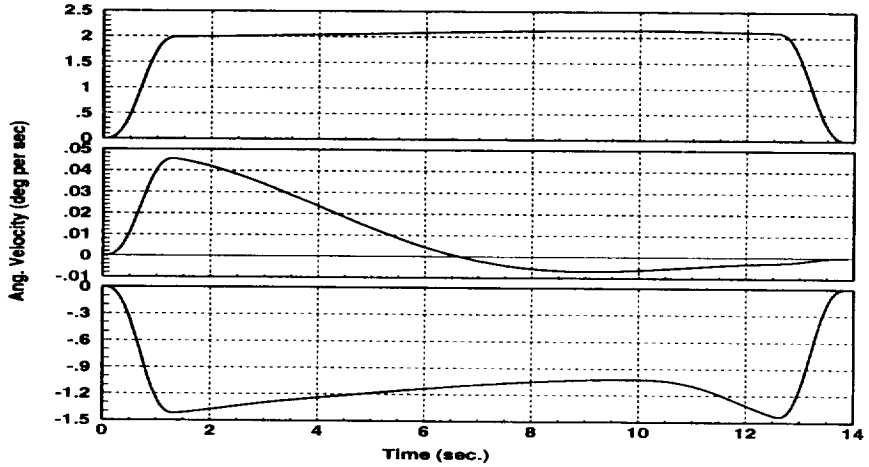

(b) Angular Velocities during Maneuver

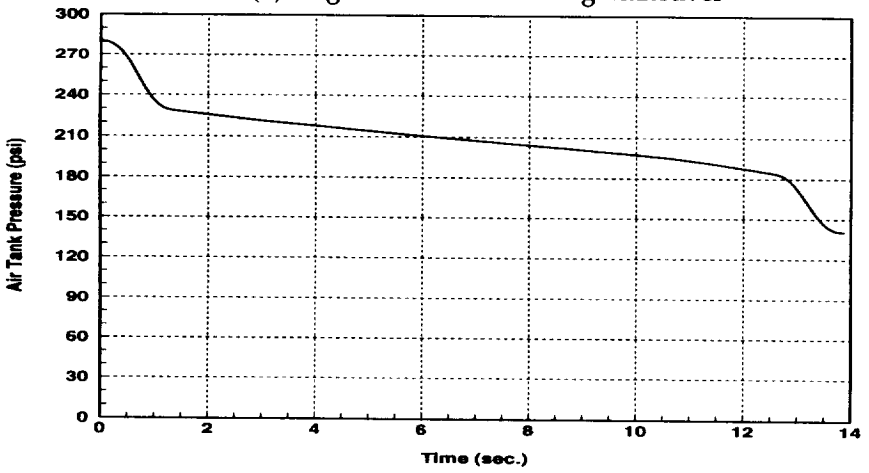

(c) Air Tank Pressure during Maneuver

Figure 4.5. States and Thrust for the 30° Yaw Maneuver Simulation (Revised Dynamics) (test23_sim_ref)

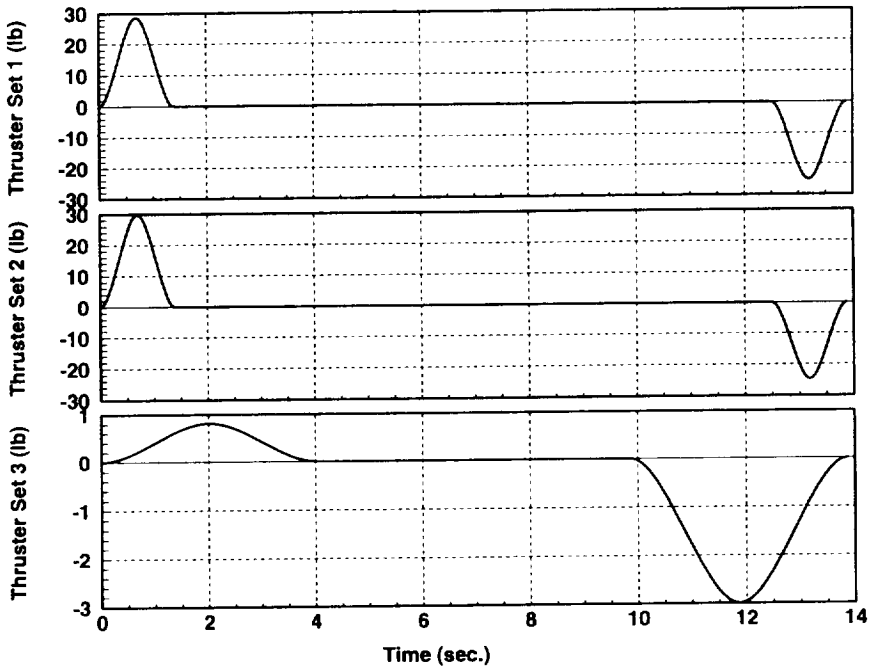

(d) Thrust during Maneuver

Figure 4.5. States and Thrust for the 30° Yaw Maneuver Simulation (Revised Dynamics) (test23_sim_ref) (cont'd)

while Figure 4.6 shows the experimental states and thrust . A comparison of these results shows that the simulation matches well with the experiment. Of course, a low frequency oscillation at the end of this maneuver still remains. However, a feedback controller will be introduced in the next section to control this problem.

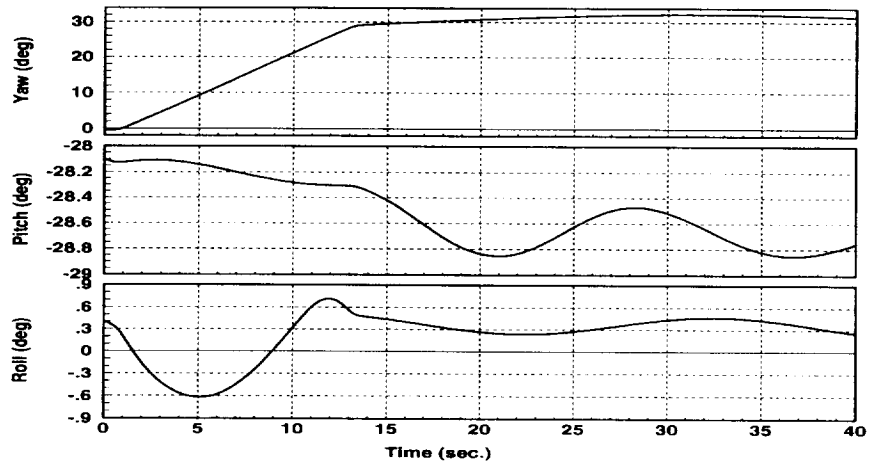

(a) Euler Angles during Maneuver

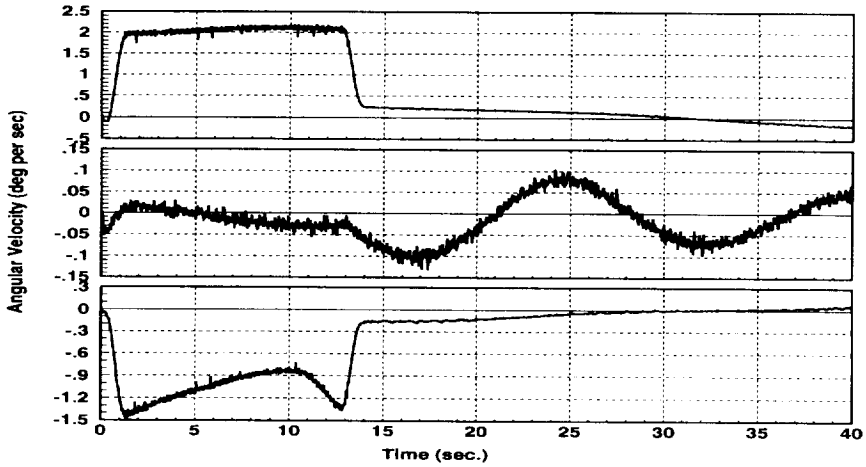

(b) Angular Velocities during Maneuver

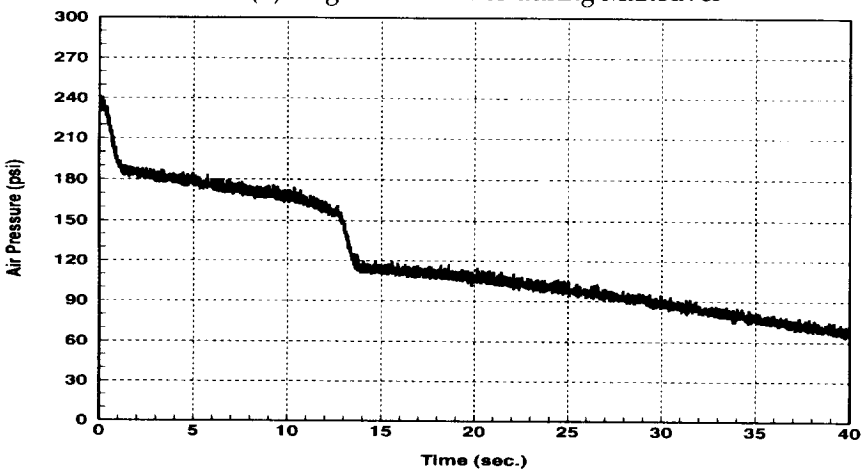

(c) Air Tank Pressure during Maneuver

Figure 4.6. States and Thrust for the 30° Yaw Maneuver Experiment (Revised Dynamics) (test23a_exp1)

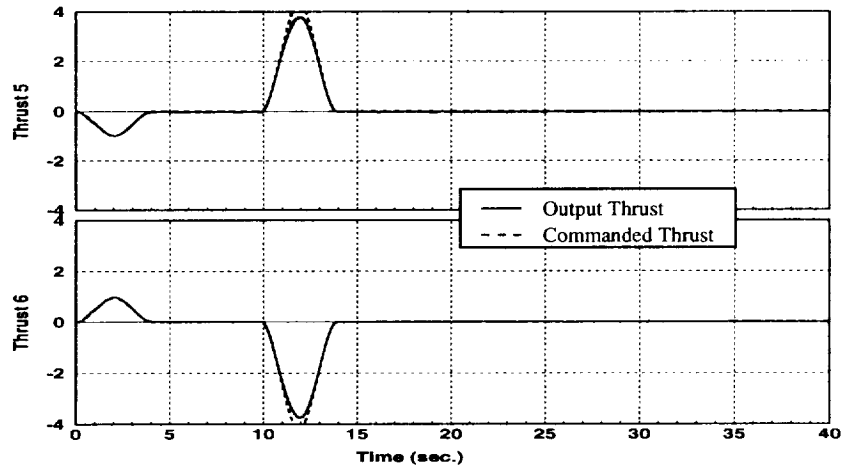

(d) Commanded & Actual Thrust during Maneuver (8 lbf Thrusters)

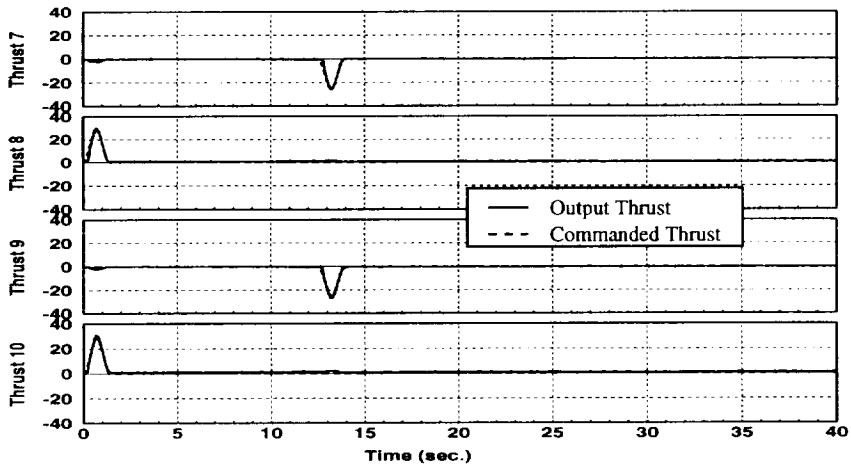

(e) Commanded & Actual Thrust during Maneuver (200 lbf Thrusters)

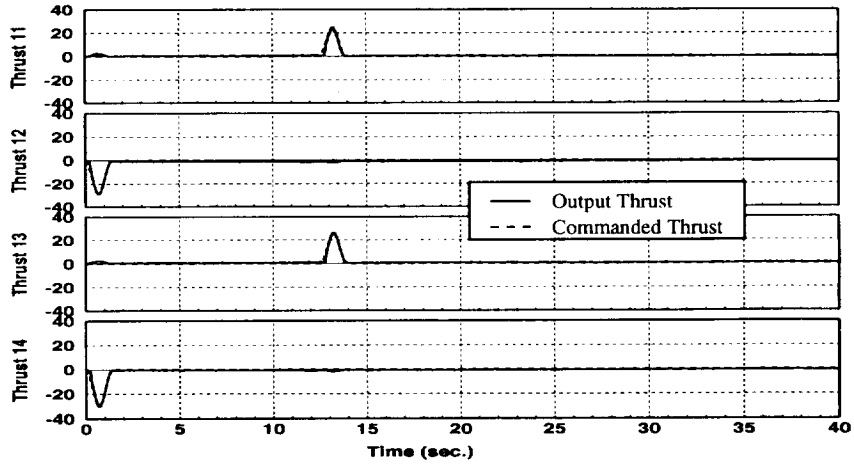

(f) Commanded & Actual Thrust during Maneuver (200 lbf Thrusters)

Figure 4.6. States and Thrust for the 30° Yaw Maneuver Experiment (Revised Dynamics) (test23a_exp1) (cont'd)

5.0. NEAR MINIMUM-TIME MANEUVERS OF THE ASTREX TEST ARTICLE WITH FINE POINTING

Using the revised dynamics model for the open-loop optimization, a bounded region around the final state is reached. However, the pitch and roll Euler angles continue to oscillate with 0.5° of the equilibrium position, while the yaw Euler angle drifts within 2° of the final state. To exactly reach the final state, the Lyapunov control laws must be used with the optimized minimum-time open-loop controls.

5.1. Near Minimum-Time Maneuvers Using a Closed-Loop Control for Fine Pointing

From Section 3.4, the final position regulator control is given by:

$$\underline{u} = -2B^{-1}\left[I\left(\omega_n{}^2 G^T\left(\underline{\beta}_f\right)\underline{\beta} + \xi\omega_n \underline{\omega}\right) + \underline{M}_{dist}\right] \tag{5.1}$$

while the tracking control is given by:

$$\underline{u} = \underline{u}_{ref} + B^{-1}\left[-2I\left(\omega_n{}^2 G^T\left(\underline{\beta}_{ref}\right)\underline{\beta} + \xi\omega_n \underline{e}_\omega\right) + \left(\tilde{\omega} I\underline{\omega} - \tilde{\omega}_{ref} I\underline{\omega}_{ref}\right) + \left(\underline{M}_{dist} - \underline{M}_{dist\,ref}\right)\right] \tag{5.2}$$

The disturbance moment in this control law will include the moment due to the displaced c.g. from the revised equations of motion:

$$\underline{M}_{dist} = -mg\,\tilde{r}_{cg}\,C_{1-2-3}(:,1) \tag{5.3}$$

while the tracking error for this disturbance moment will be given by:

$$\underline{M}_{dist} - \underline{M}_{dist\,ref} = -mg\,\tilde{r}_{cg}\left\{ C_{1-2-3}(:,1) - \left(C_{1-2-3}(:,1)\right)_{ref}\right\} \tag{5.4}$$

The moment of inertia and control influence matrices are the same used in the revised dynamics open-loop experiments in the previous section. The final pitch and roll position are determined by the c.g. position; the c.g. position was obtained experimentally from free oscillation equilibrium tests. The final Euler angle position (yaw, pitch, roll) is given by:

$$\underline{\theta}_f = [30.0 \quad -29.2 \quad 0.2]\ \text{deg.} \tag{5.5}$$

To determine the natural frequency and damping coefficients to be used, a closed-loop simulation was constructed using the SystemBuild module of the MatrixX engineering analysis software. SystemBuild is a graphical engineering analysis tool which can be used to quickly simulate complex control systems. The ASTREX test facility uses SystemBuild as a front-end interface for the data acquisition and control system in the CDAC hardware for the ASTREX structure. A major advantage of designing the closed-loop control system in a SystemBuild graphical representation is the quick integration of this control scheme into the SystemBuild data acquisition diagram at the ASTREX test facility. Figure 5.1 shows the SystemBuild Superblock which is used to simulate the final position regulation and tracking controls. From these simulations, the natural frequency and damping coefficient gains are chosen as:

$$\omega_n = 0.9 \text{ rad / sec}$$
$$\xi = 0.9 \tag{5.6}$$

Figure 5.2 shows the SystemBuild Superblock which is used to perform the data acquisition and control during the ASTREX structure maneuvers.

The 30° yaw maneuver of the ASTREX test article from the previous section was again attempted with the addition of a fine-pointing control. Using the open-loop control optimized with the revised system dynamics, two ASTREX experimental maneuvers were performed using the above Lyapunov control laws in February 1993. Figure 5.3 shows the experimental states and thrust for an optimized near minimum time maneuver with a final position regulation control. Figure 5.4 shows the states and the thrust for an optimized near minimum time maneuver with a control which tracks the reference trajectory. The closed-loop control was only applied for the first 30 seconds of the maneuver to observe the resulting dynamics.

Both of the closed-loop maneuvers come close to reaching the final equilibrium state. Unfortunately, in both of the cases, the closed loop control depletes the available air tank pressure before equilibrium is reached. In addition, the thrusters do not respond to small voltage signals during the fine-pointing stage, leading to terminal errors. The other problem is that the ASTREX test article is mounted on a near frictionless airbearing. With very little damping, the problem of exactly reaching the equilibrium state is similar to balancing an object on a knife edge. The slightest perturbation can cause an undamped oscillatory motion in the roll and pitch directions. In this set of experiments, the tracking control converges quicker than the final position regulation control primarily due to the close correspondence between the simulation and experiment. Consequently, the tracking control is better at conserving fuel than the final position regulation control.

To show that the tracking control is able to converge on the final state when a sufficient amount of fuel is available, a 10° yaw maneuver for the ASTREX structure was performed. The open-loop minimum-time yaw maneuver was optimized using the revised system dynamics and a pressure drop of only 85 psi. Figure 5.5 (a)-(g) shows the experimental states and thrust for this maneuver. The closed-loop control was again discontinued after 30 seconds. Obviously, this maneuver was able to reach the final state precisely in approximately 15 seconds. Both the Euler angles and angular velocities are essentially constant for the next 15 seconds. However, when the closed-loop control is shut off at 30 seconds, small amplitude oscillations appear primarily in the roll and pitch Euler angles. These oscillations could be caused by either vibrations introduced from the

shutdown of the thrusters or the small displacement of the gravity gradient from the equilibrium position.

The accelerometer data is given in Figure 5.5 (h). The acceleration graphs (from top to bottom) are related to the accelerometers mounted on the secondary truss measuring acceleration in the y direction of the body reference frame, mounted on the secondary truss measuring acceleration in the x-direction of the body reference frame, and mounted on the primary truss measuring acceleration in the y-direction of the body reference frame. The largest acceleration occurs as the open-loop bang-off-bang control applies acceleration and deceleration pulses at the beginning and end of the open-loop maneuver respectively.

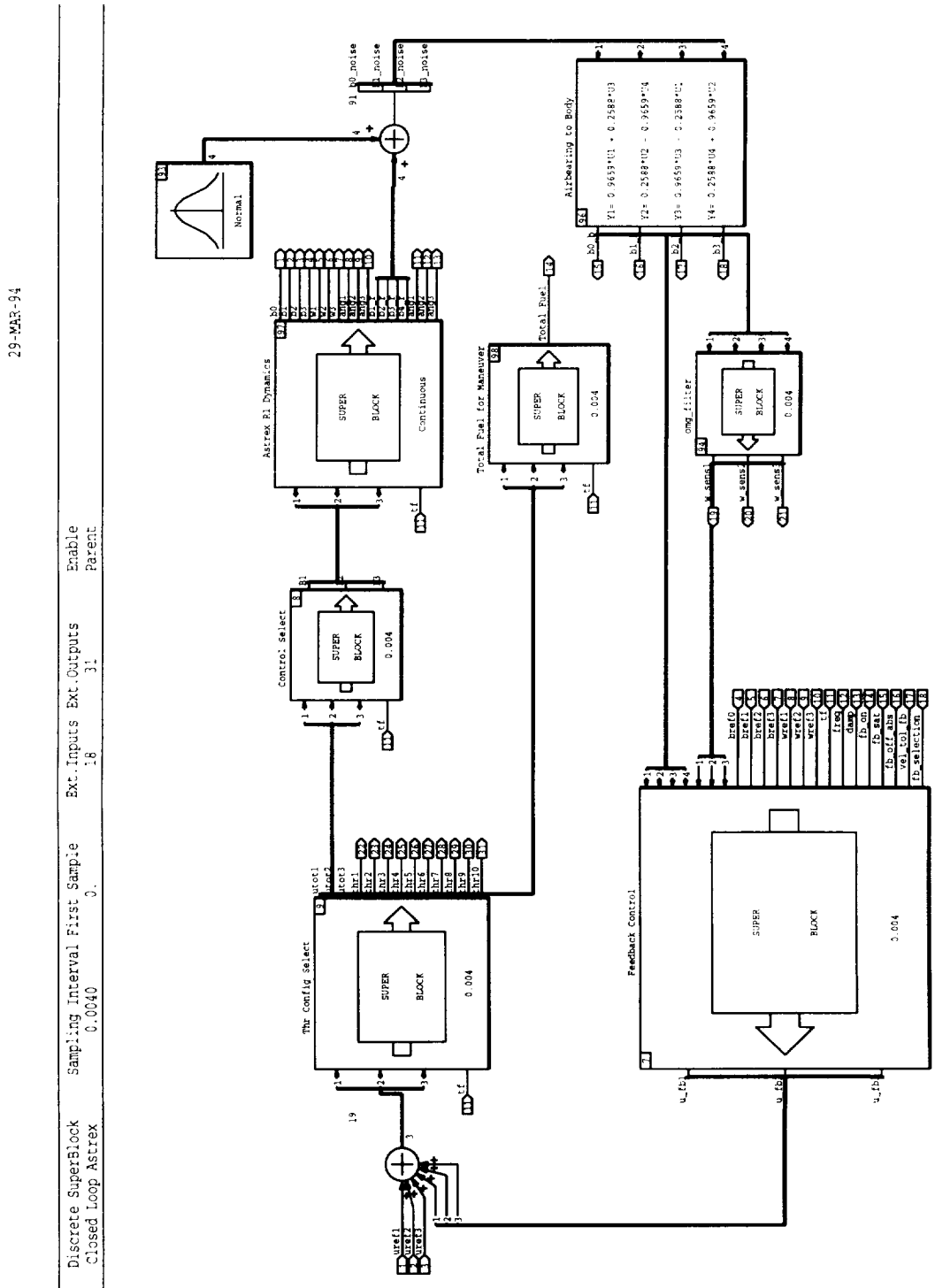

Figure 5.1. SystemBuild Superblock for Closed-Loop Control Law Simulation

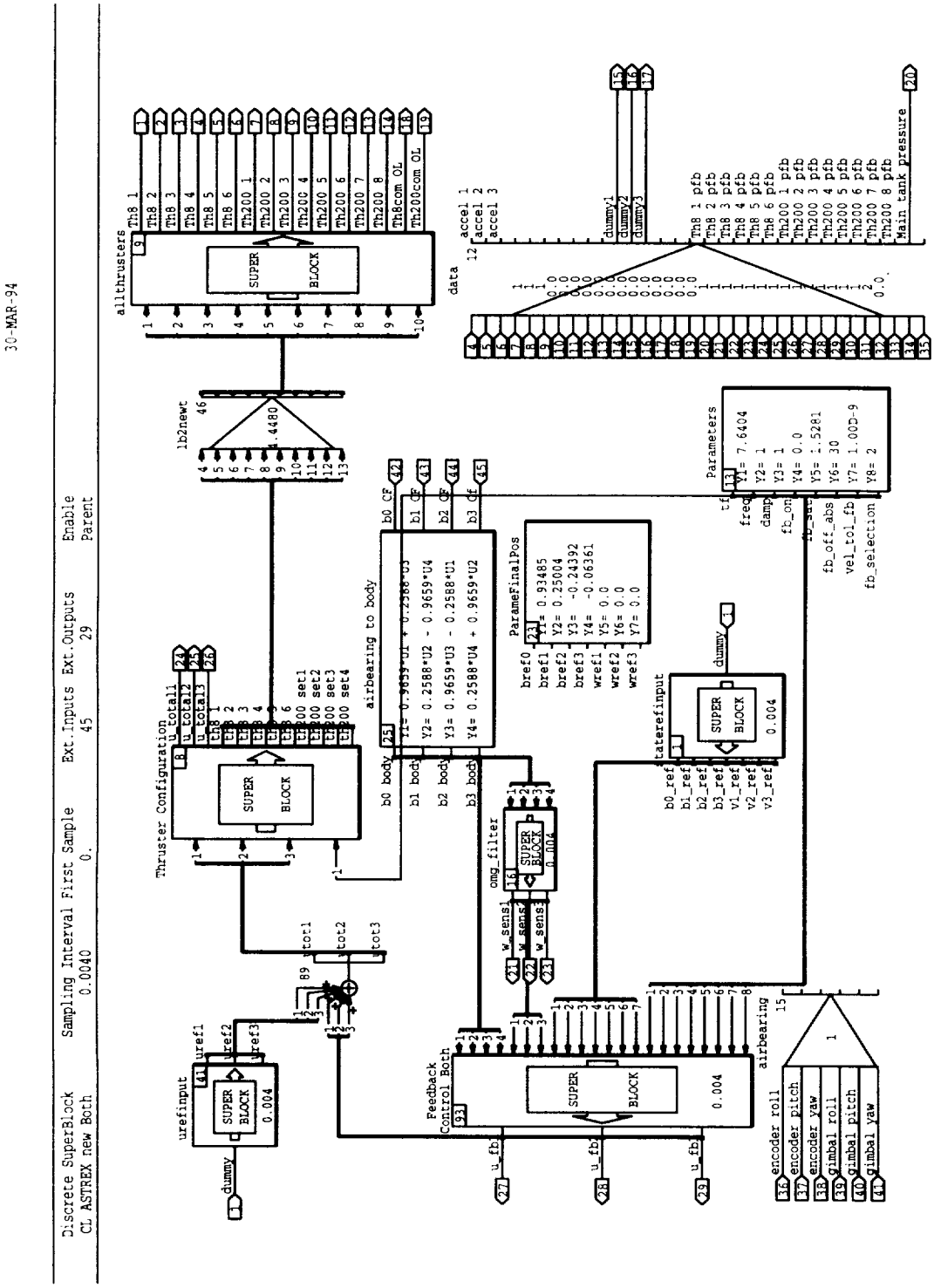

Figure 5.2. SystemBuild Superblock for Data Acquisition & Control for ASTREX Maneuvers

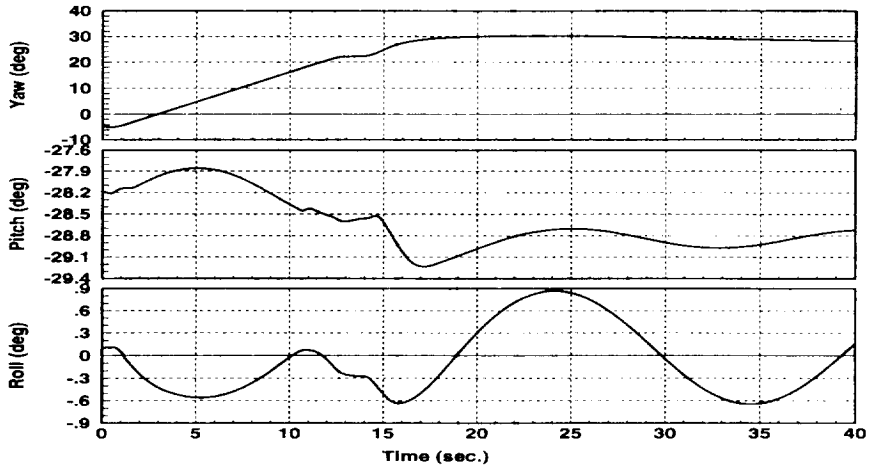

(a) Euler Angles during Maneuver

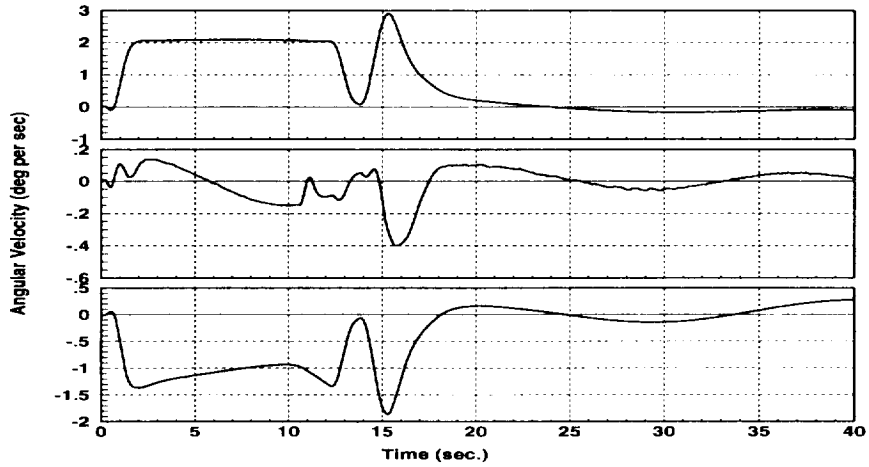

(b) Angular Velocities during Maneuver

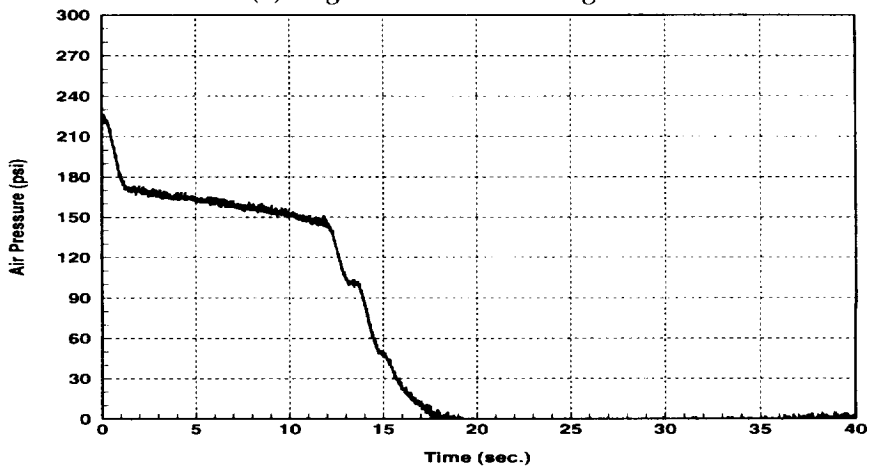

(c) Air Tank Pressure during Maneuver

Figure 5.3. Optimized Near Minimum Time 30° Yaw Maneuver with Final Position Regulation (test26b_exp1)

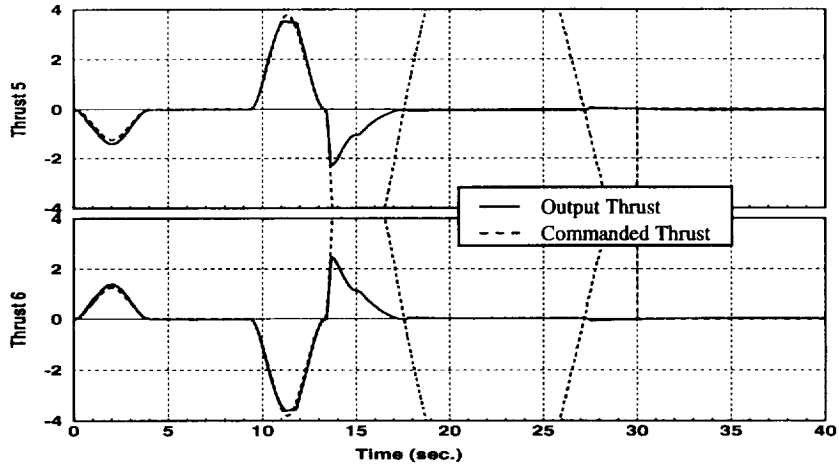

(d) Commanded & Actual Thrust during Maneuver (8 lbf Thrusters)

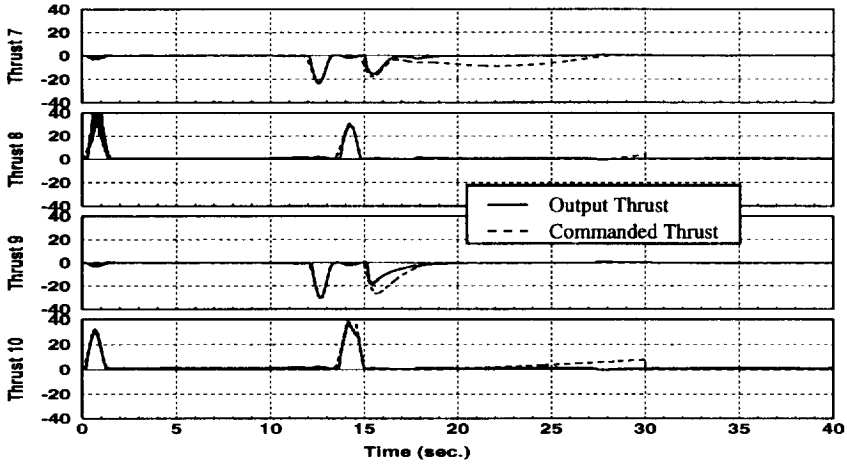

(e) Commanded & Actual Thrust during Maneuver (200 lbf Thrusters)

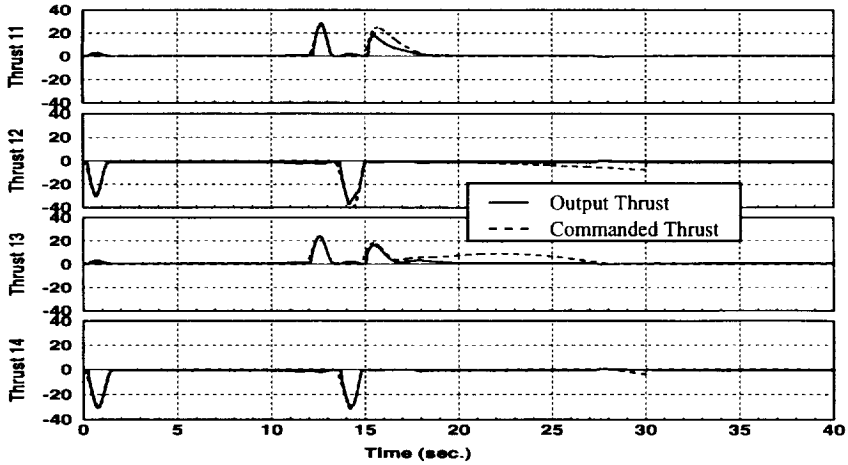

(f) Commanded & Actual Thrust during Maneuver (200 lbf Thrusters)

Figure 5.3. Optimized Near Minimum Time 30° Yaw Maneuver with Final Position Regulation (test26b_exp1) (cont'd)

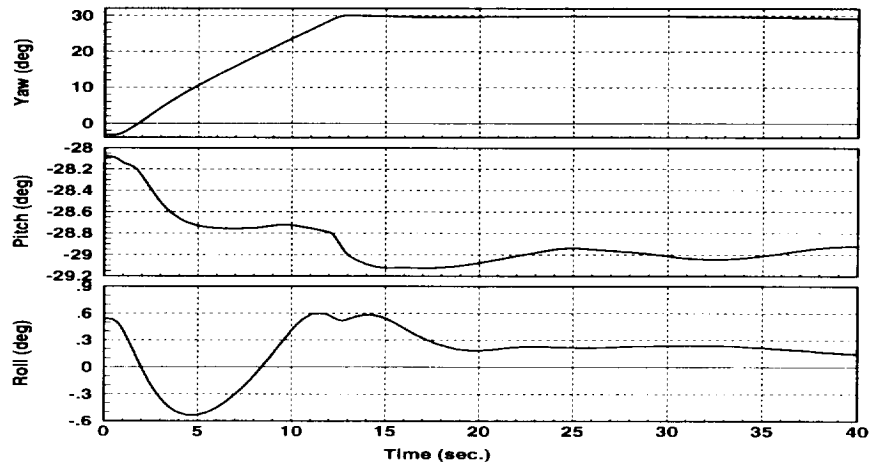

(a) Euler Angles during Maneuver

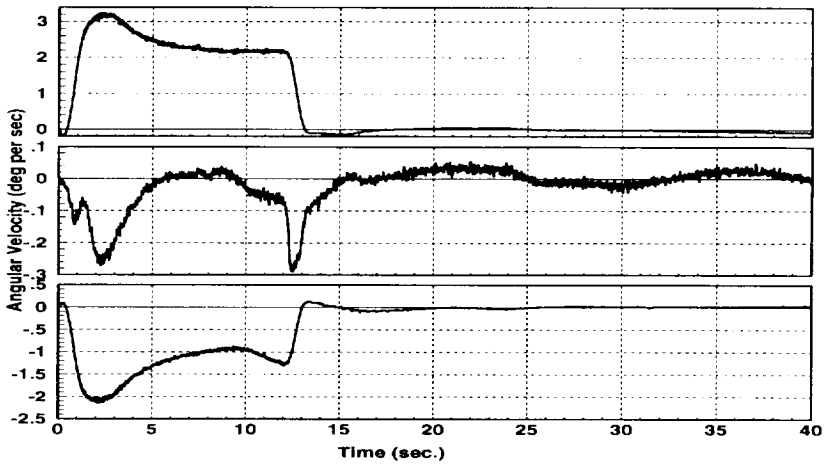

(b) Angular Velocities during Maneuver

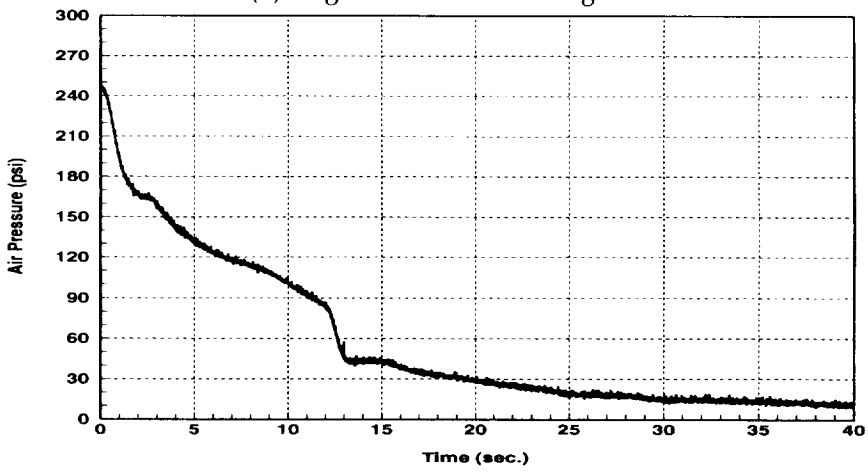

(c) Air Tank Pressure during Maneuver

Figure 5.4. Optimized Near Minimum Time 30° Yaw Maneuver with Tracking (test26c_exp1)

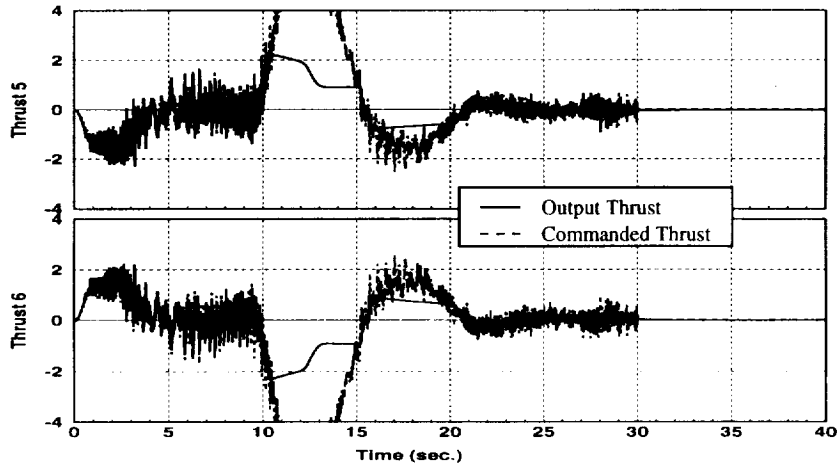

(d) Commanded & Actual Thrust during Maneuver (8 lbf Thrusters)

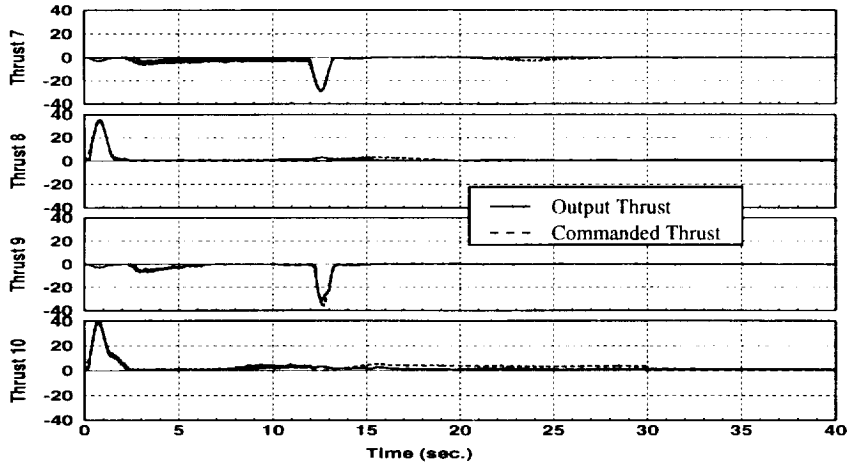

(e) Commanded & Actual Thrust during Maneuver (200 lbf Thrusters)

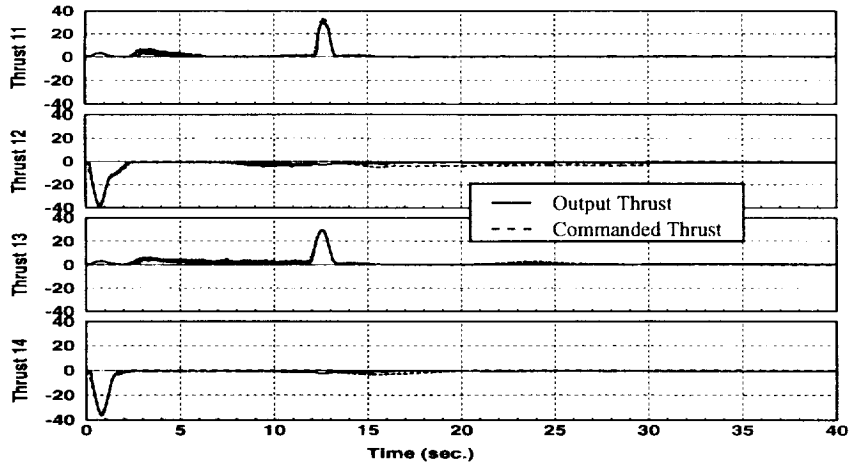

(f) Commanded & Actual Thrust during Maneuver (200 lbf Thrusters)

Figure 5.4. Optimized Near Minimum Time 30° Yaw Maneuver with Tracking (test26c_exp1) (cont'd)

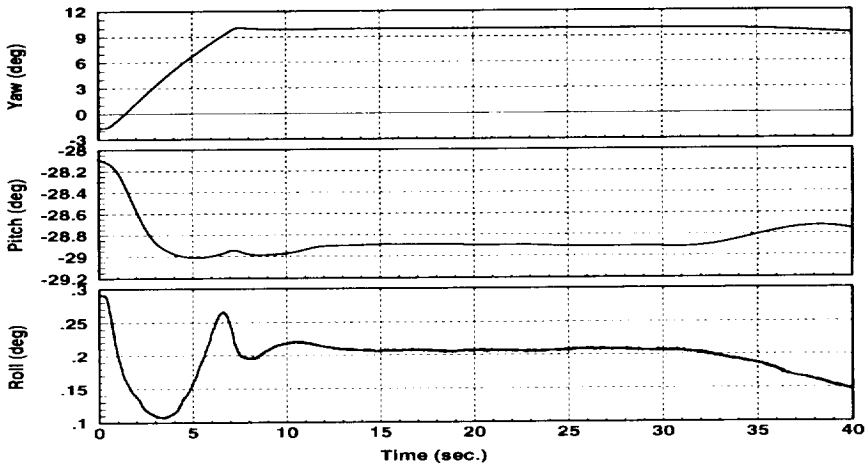

(a) Euler Angles during Maneuver

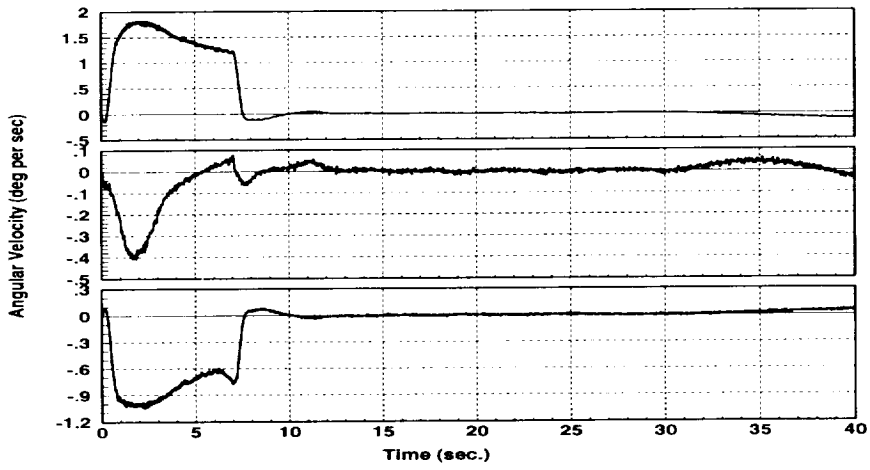

(b) Angular Velocities during Maneuver

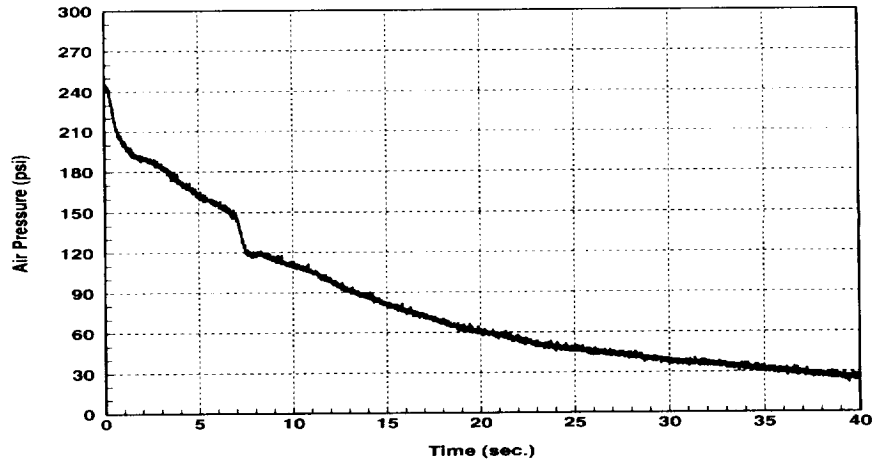

(c) Air Tank Pressure during Maneuver

Figure 5.5. Optimized Near Minimum Time 10° Yaw Maneuver with Tracking (test28_exp3)

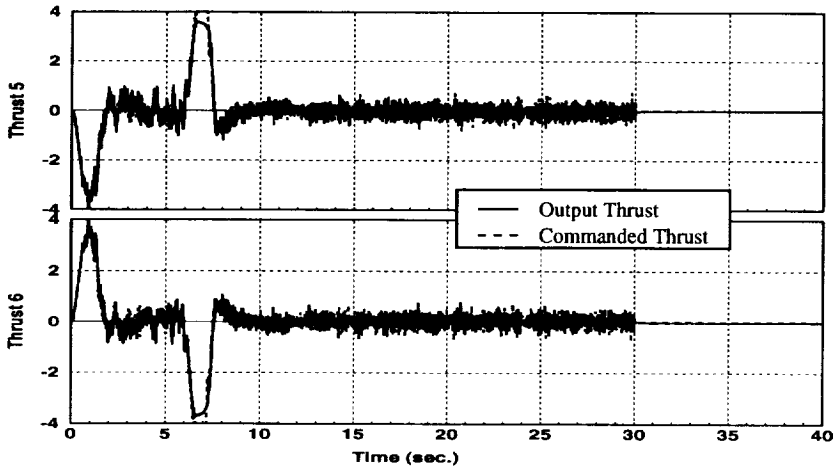

(d) Commanded & Actual Thrust during Maneuver (8 lbf Thrusters)

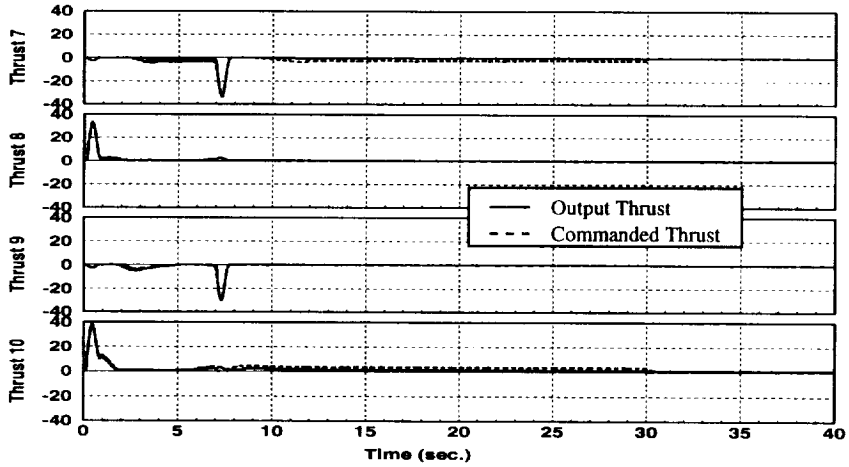

(e) Commanded & Actual Thrust during Maneuver (200 lbf Thrusters)

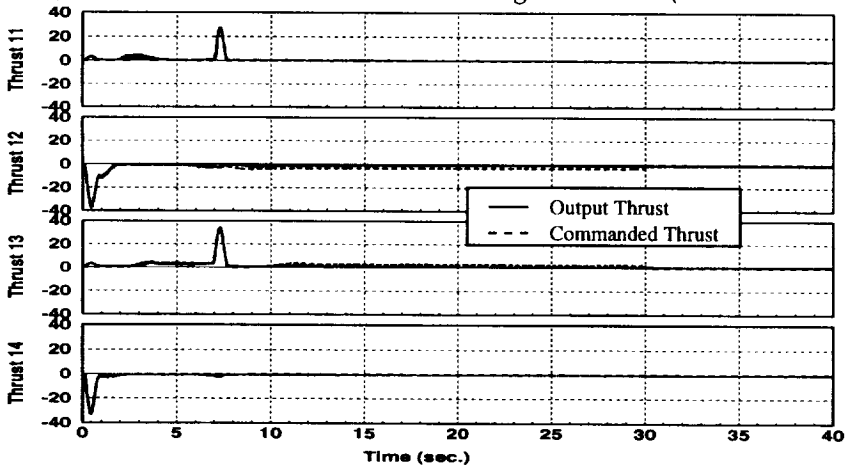

(f) Commanded & Actual Thrust during Maneuver (200 lbf Thrusters)

Figure 5.5. Optimized Near Minimum Time 10° Yaw Maneuver with Tracking (test28_exp3) (cont'd)

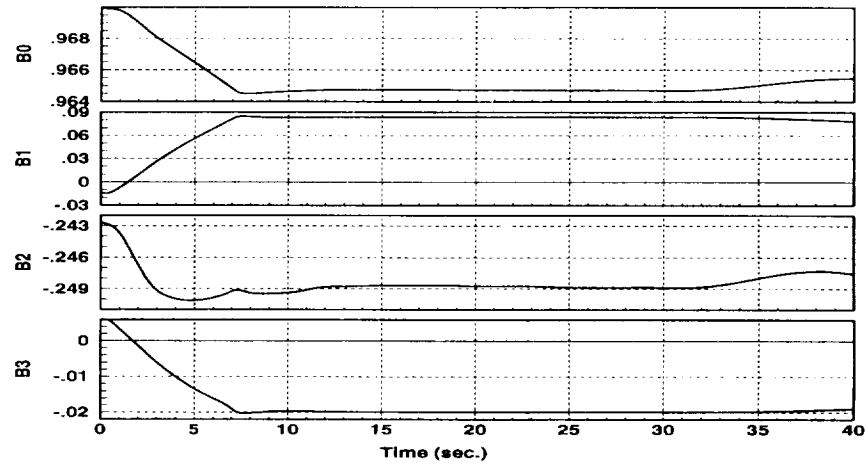

(g) Euler Parameters during Maneuver (n1 Reference Frame)

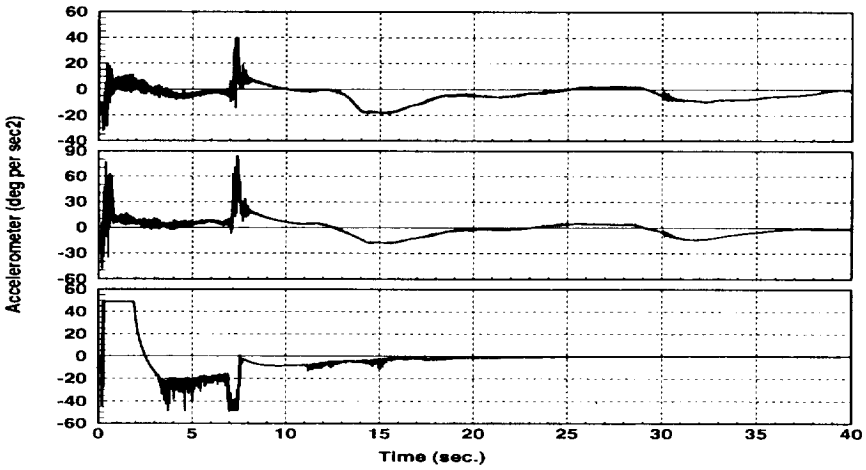

(h) Secondary Truss (x,y) & Primary Truss (y) Acceleration during Maneuver

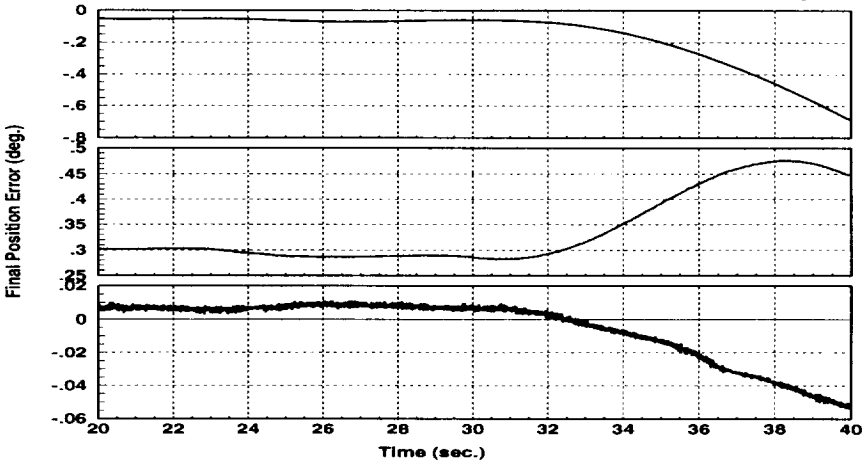

(i) Final Position Error in Euler Angles during Maneuver

Figure 5.5. Optimized Near Minimum Time 10° Yaw Maneuver with Tracking (test28_exp3) (cont'd)

6.0. CONCLUDING REMARKS & RECOMMENDATIONS

The ASTREX test facility is unique in its capabilities and features for implementing control laws for maneuvering and vibration suppression. The experiments in this report successfully demonstrated the ability of the control laws to maneuver and fine-point the structure using throttleable thrusters. The techniques implemented on the test article incorporated near minimum-time open-loop control, torque smoothing, and Lyapunov final position regulation and tracking controls. Torque-smoothing worked so well at minimizing structural excitation, that controlling the low frequency pendulum mode due to the c.g. offset became the primary concern of the investigators. The feedback control laws were implemented using attitude measurements and rates were estimated by filtering the attitude measurements.

Considerable leakage in the plumbing of the thruster system prevented "large" maneuvers from being performed. Furthermore, stray voltages in the control electronics produced erratic thruster firings leading to unacceptably large motions of the structure. To avoid possible damage to the structure, the maximum input voltage to the thrusters was limited, which consequently limited the "size" of the maneuvers. In spite of these difficulties, the control laws worked remarkably well, as shown in the experimental results.

Some suggestions for improvements and future work are given below:

1. The capacity of the compressed air tanks should be increased so that larger experimental maneuvers can be performed.
2. New rate sensors should be acquired to measure the rigid-body angular rate directly.
3. Future maneuver experiments at this facility should include both the CMGs and reaction wheels, as well as the thrusters. These tests could investigate attitude control problems such as CMG momentum management and persistent disturbance rejection.
4. Additional experiments using this testbed could validate adaptive control laws for attitude maneuvers. Indirect adaptive control laws based on estimating the inertia properties of the structure can be performed with relative ease. A mechanism to deliberately change the c.g. location might be considered to make the experiments more challenging.

7.0. REFERENCES

[1]Junkins, J.L. and Turner, J.D., *Optimal Spacecraft Rotational Maneuvers*, Elsevier Scientific, Amsterdam, Holland, 1985.

[2]Scrivener, S.L., Thompson, R.C., "Survey of Time-Optimal Attitude Maneuvers", *Journal of Guidance, Control & Dynamics*, Vol. 17, No. 2, March-April 1994, pp.225-233.

[3]Vadali, S.R., Junkins, J.L., "Optimal Open-Loop and Stable Feedback Control of Rigid Spacecraft Attitude Maneuvers", *Journal of the Astronautical Sciences*, Vol. 32, No. 2, April-June 1984, pp.105-122.

[4]Wie, B., Weiss, H., Arapostathis, A., "Quaternion Feedback Regulator for Spacecraft Eigenaxis Rotations", *Journal of Guidance*, Vol. 12, No. 3, May-June 1989, pp. 375-380.

[5]Thompson, R.C., Junkins, J.L. and Vadali, S.R., "Near-Minimum Time Open-Loop Slewing of Flexible Vehicles," *Journal of Guidance, Navigation & Control*, Vol. 12, No. 1, Jan-Feb 1989, pp. 82-88.

[6]Byers, R.M., Vadali, S.R., Junkins, J.L., "Near-Minimum Time, Closed-Loop Slewing of Flexible Spacecraft", *Journal of Guidance*, Vol. 13, No. 1, Jan.-Feb. 1990, pp. 57-65.

[7]Junkins, J.L., Rahman, Z.H., Bang, H., "Near-Minimum-Time Control of Distributed Parameter Systems: Analytical and Experimental Results", *Journal of Guidance, Control, and Dynamics*, Vol. 14, No. 2, March-April 1991, pp. 406-415.

[8]Vadali, S.R., Singh, T., Carter, T., "Computation of Near Minimum-Time Maneuvers of Flexible Structures by Parameter Optimization", *Journal of Guidance, Control & Dynamics*, Vol. 17, No. 2, March-April 1994, pp.354-360.

[9]Abhyankar, N.S., Ramakrishnan, J., et al., "Modeling, System Identification and Control of ASTREX", Paper presented at the NASA/DOD Controls-Structures Interaction Technology Conference, Lake Tahoe, NV, March 1992.

[10]Kirk, D.E., *Optimal Control Theory*, Prentice-Hall, Inc., Englewood Cliffs, NJ, 1970.

[11]Bryson, A.E. and Ho, Y.-C., *Applied Optimal Control*, Hemisphere Publishing Corp., Washington, D.C., 1975.

[12]Carter, M.T., "Near Minimum-Time Maneuvers of Large Space Structures Using Parameter Optimization and Lyapunov Feedback Control", M.S. Thesis, Aerospace Engineering, Texas A&M University, College Station, TX, Dec. 1993.

[13]Mukherjee, R., Chen, D., "An Asymptotic Stability Theorem for Autonomous Systems", *Journal of Guidance, Control & Dynamics*, Vol. 16, No. 5, Sept-Oct 1993, pp. 961-962.

APPENDIX A

Near Minimum-Time Maneuver Experiments on the ASTREX Test Article

Table A-1. Attitude Reference Maneuver Test History for the ASTREX Structure

Test #	Test Description	Control Profile	Desired Initial & Final Euler Angle (deg.)	Thruster Combination (Yaw, Pitch, Roll) (lb.)	Initial Pressure (psi)	Desired Pressure Drop (psi)	c.g. Effect	Spring Effect	Damping Effect
5	50° Yaw Maneuver	BOB (Carter)	[0.0 −30.0 0.0] [50.0 −30.0 0.0]	[8 8 8]	---	140.9			
6	50° Yaw Maneuver	BOB (Bell)	[0.0 −30.0 0.0] [50.0 −30.0 0.0]	[200 200 8]	---	~220.0			
6a	50° Yaw Maneuver	BOB (Bell)	[0.0 −30.0 0.0] [50.0 −30.0 0.0]	[200 200 8]	---	149.2			
6b	50° Yaw Maneuver	BB (Bell)	[0.0 −30.0 0.0] [50.0 −30.0 0.0]	[200 200 8]	---	92.2			
7	50° Yaw Maneuver	BB (Carter)	[0.0 −30.0 0.0] [50.0 −30.0 0.0]	[200 200 8]	---	250.0			
8	50° Yaw Maneuver	BB (Carter)	[0.0 −30.0 0.0] [50.0 −30.0 0.0]	[8 8 8]	---	109.1			
9	50° Yaw Maneuver	BB (Carter)	[0.0 −30.0 0.0] [50.0 −30.0 0.0]	[200 200 8]	---	149.9			
12	30° Yaw Maneuver	BOB (Carter)	[0.0 −30.0 0.0] [30.0 −30.0 0.0]	[200 200 8]	250.0	100.0			
13	60° Yaw Maneuver	BOB (Carter)	[0.0 −30.0 0.0] [60.0 −30.0 0.0]	[200 200 8]	250.0	100.0			
15	30° Yaw Maneuver	BOB (Carter)	[0.0 −30.0 0.0] [30.0 −30.0 0.0]	[200 200 8]	250.0	130.0		X	

Table A-1 (cont'd). Attitude Reference Maneuver Test History for the ASTREX Structure

Test #	Test Description	Control Profile	Desired Initial & Final Euler Angle (deg.)	Thruster Combination (Yaw, Pitch, Roll) (lb.)	Initial Pressure (psi)	Desired Pressure Drop (psi)	c.g. Effect	Spring Effect	Damping Effect
16	30° Yaw Maneuver	BOB (Carter)	[0.0 −30.0 0.0] [30.0 −30.0 0.0]	[200 200 8]	250.0	130.0		X	
17	30° Yaw Maneuver	BOB (Carter)	[0.0 −30.0 0.0] [30.0 −30.0 0.0]	[200 200 8]	250.0	130.0		X	
18	30° Yaw Maneuver	BOB (Carter)	[0.0 −30.0 0.0] [30.0 −30.0 0.0]	[200 200 8]	280.0	140.0		X	
19	30° Yaw Maneuver	BOB (Carter)	[0.0 −30.0 0.0] [30.0 −30.0 0.0]	[200 200 8]	280.0	140.0		X	
20	30° Yaw Maneuver	BOB (Carter)	[0.0 −30.0 0.0] [30.0 −30.0 0.0]	[200 200 8]	280.0	140.0		X	
21	30° Yaw Maneuver	BOB (Carter)	[0.0 −30.0 0.0] [30.0 −30.0 0.0]	[200 200 8]	280.0	140.0		X	
23	30° Yaw Maneuver	BOB (Carter)	[0.0 −30.0 0.0] [30.0 −30.0 0.0]	[200 200 8]	280.0	140.0	X		
24	Final Position Regulation	---	--- [0.0 −30.0 0.0]	[200 200 8]	---	---			
25	Final Position Regulation	---	--- [0.0 −30.0 0.0]	[8 8 8]	---	---			

Table A-1 (cont'd). Attitude Reference Maneuver Test History for the ASTREX Structure

Test #	Test Description	Control Profile	Desired Initial & Final Euler Angle (deg.)	Thruster Combination (Yaw, Pitch, Roll) (lb.)	Initial Pressure (psi)	Desired Pressure Drop (psi)	c.g. Effect	Spring Effect	Damping Effect
26	30° Yaw Maneuver	BOB (Carter)	[0.0 −29.2 0.2] [30.0 −29.2 0.2]	[200 200 8] Open-Loop [8 8 8] Closed-Loop	260.0	140.0	X		X
27	Final Position Regulation	---	--- [0.0 −29.2 0.2]	[200 200 8]	---	---	X		
28	10° Yaw Maneuver	BOB (Carter)	[0.0 −29.2 0.2] [10.0 −29.2 0.2]	[200 200 8]	260.0	85.0	X		X

Table A-2. Attitude Maneuver Test History for the ASTREX Structure

Test #	Test Description	Experiment #	Date	Open Loop	Closed Loop	Correct n2 to n1 Transformation	Euler Parameter Digital Filter	Closed-Loop Controller
Experimental Measurements: $\underline{\beta}$, $\underline{\omega}$, $\underline{T}_{pfb}$								
5	50° Yaw Maneuver	1 2	1/29/93 2/4/93	X			$\frac{7.3851(z^2-1)}{z^2-1.4560z+0.5300}$	
Experimental Measurements: $\underline{\beta}$, $\underline{\omega}$, $\underline{T}_{pfb}$, $\dot{V}$								
6	50° Yaw Maneuver	1	2/4/93	X			$\frac{7.3851(z^2-1)}{z^2-1.4560z+0.5300}$	
6a	50° Yaw Maneuver	1	3/1/93	X			$\frac{7.3851(z^2-1)}{z^2-1.4560z+0.5300}$	
6b	50° Yaw Maneuver	1 2	3/1/93	X			$\frac{7.3851(z^2-1)}{z^2-1.4560z+0.5300}$	
7	50° Yaw Maneuver	1 2	3/1/93 4/12/93	X			$\frac{7.3851(z^2-1)}{z^2-1.4560z+0.5300}$	
8	50° Yaw Maneuver	1 2	3/1/93 4/12/93	X			$\frac{7.3851(z^2-1)}{z^2-1.4560z+0.5300}$	
9	50° Yaw Maneuver	1	4/12/93	X			$\frac{7.3851(z^2-1)}{z^2-1.4560z+0.5300}$	
12	30° Yaw Maneuver	1	4/26/93	X			$\frac{7.3851(z^2-1)}{z^2-1.4560z+0.5300}$	

Table A-2 (cont'd). Attitude Maneuver Test History for the ASTREX Structure

Test #	Test Description	Experiment #	Date	Open Loop	Closed Loop	Correct **n2** to **n1** Transformation	Euler Parameter Digital Filter	Closed-Loop Controller
Experimental Measurements: $\underline{\beta}$, $\underline{\omega}$, $\underline{T}_{pfb}$, $\dot{V}$								
13	60° Yaw Maneuver	1	4/19/93	X			$\frac{7.3851(z^2-1)}{z^2-1.4560z+0.5300}$	
15	30° Yaw Maneuver	1	7/15/93	X			$\frac{9.2313(z^2-1)}{z^2-1.4560z+0.5299}$	
16	30° Yaw Maneuver	1	8/6/93	X			$\frac{9.2313(z^2-1)}{z^2-1.4560z+0.5299}$	
17	30° Yaw Maneuver	1 2	8/10/93 8/10/93	X			$\frac{9.2313(z^2-1)}{z^2-1.4560z+0.5299}$	
18	30° Yaw Maneuver	1 2 3	8/18/93 8/27/93 8/29/93	X			$\frac{9.2313(z^2-1)}{z^2-1.4560z+0.5299}$	
19	30° Yaw Maneuver	1 2 3	9/6/93 9/8/93 9/8/93	X			$\frac{9.2313(z^2-1)}{z^2-1.4560z+0.5299}$	
20	30° Yaw Maneuver	1 2 3 4	9/23/93 9/23/93 10/2/93 10/8/93	X			$\frac{9.2313(z^2-1)}{z^2-1.4560z+0.5299}$	
21a	30° Yaw Maneuver	1	10/8/93	X			$\frac{9.2313(z^2-1)}{z^2-1.4560z+0.5299}$	

Table A-2 (cont'd). Attitude Maneuver Test History for the ASTREX Structure

Test #	Test Description	Experi-ment #	Date	Open Loop	Closed Loop	Correct **n2** to **n1** Tranform -ation	Euler Parameter Digital Filter	Closed-Loop Controller
Experimental Measurements: $\underline{\beta}, \underline{\omega}, \underline{T}_{pfb}, \dot{V}, \underline{\ddot{\theta}}$								
26c	30° Yaw Maneuver	1 2	2/2/94 2/3/94	X	X	X	$\frac{2.7172\left(z^2-1\right)}{z^2-1.6554\,z+0.6774}$	Tracking $\omega_n = 0.9,\ \xi = 0.9$
27	Final Position Regulation	1 2	1/28/94 2/2/94		X	X	$\frac{0.0790\left(z^2-1\right)}{z^2-1.9504\,z+0.9510}$	Final Pos. Regulation $\omega_n = 0.9,\ \xi = 0.9$
28	10° Yaw Maneuver	1 2 3	2/15/94 2/15/94 2/15/94	X	X	X	$\frac{2.7172\left(z^2-1\right)}{z^2-1.6554\,z+0.6774}$	Tracking $\omega_n = 0.9,\ \xi = 0.9$

Table A-2 (cont'd). Attitude Maneuver Test History for the ASTREX Structure

Test #	Test Description	Experiment #	Date	Open Loop	Closed Loop	Correct **n2** to **n1** Transformation	Euler Parameter Digital Filter	Closed-Loop Controller
Experimental Measurements: $\underline{\beta}, \underline{\omega}, \underline{T}_{pfb}, \dot{V}$								
21b	30° Yaw Maneuver	1 2	11/15/93 11/15/93	X	X		$\frac{9.2313\left(z^2-1\right)}{z^2-1.4560z+0.5299}$	Final Pos. Regulation $\omega_n = 0.8,\ \xi = 0.8$
Experimental Measurements: $\underline{\beta}, \underline{\omega}, \underline{T}_{pfb}, \dot{V}, \underline{\ddot{\theta}}$								
23a	30° Yaw Maneuver	1	12/3/93	X			$\frac{28.09\left(z^2-1\right)}{z^2-0.9705z+0.1952}$	
23b	30° Yaw Maneuver	1	12/1/93	X	X		$\frac{28.09\left(z^2-1\right)}{z^2-0.9705z+0.1952}$	Final Pos. Regulation $\omega_n = 0.9,\ \xi = 0.9$
24	Final Position Regulation	1	12/1/93		X		$\frac{28.09\left(z^2-1\right)}{z^2-0.9705z+0.1952}$	Final Pos. Regulation $\omega_n = 0.9,\ \xi = 0.9$
25	Final Position Regulation	1 2	12/8/93 12/8/93		X		$\frac{28.09\left(z^2-1\right)}{z^2-0.9705z+0.1952}$	Final Pos. Regulation $\omega_n = 0.9,\ \xi = 0.9$
26a	30° Yaw Maneuver	1 2 3 4	1/14/94 1/19/94 1/20/94 1/21/94	X			$\frac{28.09\left(z^2-1\right)}{z^2-0.9705z+0.1952}$	
26b	30° Yaw Maneuver	1	1/28/94	X	X	X	$\frac{0.0790\left(z^2-1\right)}{z^2-1.9504z+0.9510}$	Final Pos. Regulation $\omega_n = 0.9,\ \xi = 0.9$

Table A-3. Equilibrium Test History for the ASTREX Structure

Test #	Test Description	Experiment #	Date	Experiment Duration (sec)	Mean Pitch Euler Angle (deg.)	Mean Roll Euler Angle (deg.)
1	Initial Pitch Displacement (around 0° Yaw)	1	12/7/93	100.0	-29.24	0.23
2	Initial Roll Displacement (around 0° Yaw)	1	12/7/93	160.0	-29.18	0.33
3	Initial Pitch Displacement (around 65° Yaw)	1	12/7/93	100.0	-29.15	0.29
4	Initial Roll Displacement (around 65° Yaw)	1	12/7/93	160.0	-29.19	0.29

Table A-4. Pressure Leakage Test History for the ASTREX Structure

Test #	Test Description	Experiment #	Date	Experiment Duration (sec)	Initial Pressure (psi)	Pressure Leakage Constant ($in^2/lb\text{-}sec^{-1}$)
1	Zero-Thrust Pressure Leakage Test	1	7/15/93	50.0	304.15	6.26e-5

REPORT DOCUMENTATION PAGE

Form Approved
OMB No. 0704-0188

1. AGENCY USE ONLY *(Leave blank)*	2. REPORT DATE	3. REPORT TYPE AND DATES COVERED
	August 1994	Contractor Report

4. TITLE AND SUBTITLE
Near Minimum-Time Maneuvers of the Advanced Space Structures Technology Research Experiment (ASTREX) Test Article: Theory and Experiments

5. FUNDING NUMBERS
C NAS1-19373
WU 590-14-91-52

6. AUTHOR(S)
Srinivas R. Vadali and Michael T. Carter

7. PERFORMING ORGANIZATION NAME(S) AND ADDRESS(ES)
Texas A&M University
Department of Aerospace Engineering
College Station, TX 77843-3141

8. PERFORMING ORGANIZATION REPORT NUMBER

9. SPONSORING/MONITORING AGENCY NAME(S) AND ADDRESS(ES)
National Aeronautics and Space Adminsitration
Langley Research Center
Hampton, VA 23681-0001

10. SPONSORING/MONITORING AGENCY REPORT NUMBER
NASA CR-4616

11. SUPPLEMENTARY NOTES
Langley Technical Monitor: Rudeen Smith-Taylor
Final Report

12a. DISTRIBUTION/AVAILABILITY STATEMENT
Unclassified-Unlimited
Subject Category 18

12b. DISTRIBUTION CODE

13. ABSTRACT *(Maximum 200 words)*
The Phillips Laboratory at the Edwards Air Force Base has developed the Advanced Space Structures Technology Research Experiment (ASTREX) facility to serve as a testbed for demonstrating the applicability of proven theories to the challenges of spacecraft maneuvers and structural control. This report describes the work performed on the ASTREX test article by Texas A&M University under contract NAS1-19373 as a part of the Control-Structure Interaction (CSI) Guest Investigator Program. The focus of this work is on maneuvering the ASTREX test article with compressed air thrusters that can be throttled, while attenuating structural excitation. The theoretical foundation for designing the near minimum-time thrust commands is based on the generation of smooth, parameterized optimal open-loop control profiles, and the determination of control laws for final position regulation and tracking using Lyapuniv stability theory. Details of the theory, mathematical modeling, model updating and compensation for the presence of "real world" effects are described and the experimental results are presented. The results show an excellent match between theory and experiments.

14. SUBJECT TERMS
Controls-Structures Interaction, Ground-based Experiment, Torque-Smoothing, Near-Minimum-Time Manuvers

15. NUMBER OF PAGES
72

16. PRICE CODE
A04

17. SECURITY CLASSIFICATION OF REPORT	18. SECURITY CLASSIFICATION OF THIS PAGE	19. SECURITY CLASSIFICATION OF ABSTRACT	20. LIMITATION OF ABSTRACT
Unclassified	Unclassified		